JGR Biogeosciences

RESEARCH ARTICLE
10.1029/2020JG005713

Changes in Sedimentary Phosphorus Burial Following Artificial Eutrophication of Lake 227, Experimental Lakes Area, Ontario, Canada

D. W. O'Connell[1,2], N. Ansems[3,4], R. K. Kukkadapu[5], D. Jaisi[6], D. M. Orihel[7], B. J. Cade-Menun[8], Y. Hu[9], J. Wiklund[10], R. I. Hall[10], H. Chessell[2], T. Behrends[4], and P. Van Cappellen[2]

[1]Department of Civil, Structural and Environmental Engineering, Trinity College Dublin, Dublin 2, Ireland, [2]Water Institute, Ecohydrology Research Group, University of Waterloo, Waterloo, Ontario, Canada, [3]Soil Geography and Landscape Group, Wageningen University, Wageningen, The Netherlands, [4]Department of Earth Sciences, Faculty of Geosciences, Utrecht University, Utrecht, The Netherlands, [5]Environmental Molecular Sciences Laboratory, Pacific Northwest National Laboratory, Richland, WA, USA, [6]Department of Plant and Soil Science, University of Delaware, Newark, DE, USA, [7]School of Environmental Studies, Queen's University, Kingston, Ontario, Canada, [8]Swift Current Research and Development Centre, Agriculture and Agri-Food Canada, Swift Current, Saskatchewan, Canada, [9]Canadian Light Source, Saskatoon, Saskatchewan, Canada, [10]Department of Biology, University of Waterloo, Waterloo, Ontario, Canada

Key Points:

- Since 1969, phosphorus (P) has been continuously added to Lake 227, causing large increases in the sediment accumulations of organic (P_{Org}) and $NaHCO_3$-extractable P (P_{Hum})
- P_{Hum} comprises ternary phosphate-metal-humic complexes with Fe (III) as one of the bridging metal cations
- Sediments of Lake 227 harbor a large legacy of reactive P, which may fuel internal P loading to the water column once artificial fertilization is terminated

Supporting Information:

- Supporting Information S1

Correspondence to:
D. W. O'Connell,
david.oconnell@tcd.ie

Citation:
O'Connell, D. W., Ansems, N., Kukkadapu, R. K., Jaisi, D., Orihel, D. M., Cade-Menun, B. J., et al. (2020). Changes in sedimentary phosphorus burial following artificial eutrophication of Lake 227, Experimental Lakes Area, Ontario, Canada. *Journal of Geophysical Research: Biogeosciences*, *125*, e2020JG005713. https://doi.org/10.1029/2020JG005713

Received 22 FEB 2020
Accepted 2 JUN 2020
Accepted article online 11 JUN 2020
Corrected 5 NOV 2020

This article was corrected on 5 NOV 2020. See the end of the full text for details.

Author Contributions:
Conceptualization: D. W. O'Connell, P. Van Cappellen
Formal analysis: D. W. O'Connell, N. Ansems, R. K. Kukkadapu, D. Jaisi, B. J.
(continued)

Abstract Lake 227 of the Experimental Lakes Area (ELA) in Ontario, Canada, has been fertilized with phosphorus (P) since 1969, which resulted in a rapid transition from oligotrophic to eutrophic conditions. Sediment cores collected from the oxygenated epilimnion, and the mostly anoxic hypolimnion of this unique lake contain a historical record of the changes in sediment P speciation and burial rates across the trophic transition. To elucidate these changes, results of chemical extractions were combined with ^{210}Pb sediment dating, and with ^{31}P NMR, Mössbauer, and XANES spectroscopies. Prior to 1969, organic P (P_{Org}) was the major sedimentary P sink in Lake 227. Eutrophication of the lake coincided with marked increases in the burial rate of total P (TP), as well as in the relative contribution of the $NaHCO_3$-extractable P pool (humic-bound P, P_{Hum}). Together, P_{Hum} and P_{Org} account for ≥70% of total P burial in the sediments deposited since artificial fertilization started. The P_{Hum} fraction likely comprises phosphate complexes with humic substances. The strong linear correlation between P and iron (Fe) extracted by $NaHCO_3$ implies a close association of the two elements in the humic fraction. Mössbauer and XANES spectra further indicate that most Fe in the post-1969 sediments remained in the Fe (III) oxidation state, which is attributed to the stabilization of reducible Fe by organic matter, in part via the formation of phosphate-Fe (III)-humic complexes. Importantly, our results show that the eutrophication experimentation of Lake 227 caused the accumulation of a large reservoir of reactive sediment P, which may continue to fuel internal P loading to the water column once artificial fertilization is terminated.

1. Introduction

Strict environmental regulations in many countries have contributed to substantial decreases in external phosphorus (P) loading to lakes from agriculture and urban activities. Nevertheless, many eutrophic lakes have not shown the expected improvement in water quality following a reduction in external P sources. Internal loading of legacy P from lake sediments (i.e., benthic recycling) may in part be responsible for the delayed recovery of many of these lakes (Jeppesen et al., 2005). In addition, a reduction in external P supply may actually amplify the role of internal P loading (Van der Molen & Boers, 1994). Our understanding of nutrient loading and the associated effects on lake primary productivity, thus, depends on a detailed understanding of the cycling of P at the sediment-water interface (SWI).

Because of the importance of internal P loading in lentic ecosystems, many studies have investigated the factors that affect benthic P release (Ahlgren et al., 2006; Orihel et al., 2017; Søndergaard et al., 2002). Phosphorus cycling in aquatic sediments is usually explained with the classic (Mortimer, 1941) model, where P release from sediments is controlled largely by the oxidation-reduction cycle of iron (Fe). This model is based on the strong affinity of phosphate anions ($H_2PO_4^-$ or HPO_4^{2-} in the natural pH range of

Cade-Menun, Y. Hu, J. Wiklund, H. Chessell
Funding acquisition: T. Behrends, P. Van Cappellen
Investigation: D. W. O'Connell, N. Ansems, R. K. Kukkadapu, D. Jaisi, B. J. Cade-Menun, Y. Hu, H. Chessell
Methodology: D. W. O'Connell, N. Ansems, R. K. Kukkadapu
Project administration: D. W. O'Connell, P. Van Cappellen
Resources: D. Jaisi
Supervision: D. W. O'Connell
Validation: D. W. O'Connell, N. Ansems, D. Jaisi, B. J. Cade-Menun, Y. Hu
Visualization: D. W. O'Connell, N. Ansems
Writing - original draft: D. W. O'Connell, N. Ansems, R. K. Kukkadapu, Y. Hu, J. Wiklund, P. Van Cappellen
Writing – review & editing: D. W. O'Connell, N. Ansems, R. K. Kukkadapu, D. Jaisi, B. J. Cade-Menun, Y. Hu, R. I. Hall, P. Van Cappellen

most lakes) for ferric Fe [Fe (III)] oxyhydroxide minerals. When the pore water redox potential drops sufficiently, solid Fe (III) oxyhydroxides reductively dissolve, releasing soluble ferrous Fe [Fe (II)] and sorbed phosphate to the pore waters. Sulfate (SO_4^{2-})-controlled phosphate mobilization has been suggested as an alternative, but related, P-release mechanism (Gächter & Müller, 2003). In sulfate-rich aquatic sediments, production of sulfide (S^{2-}) converts Fe (III) phases into ferrous sulfide minerals, hence limiting the sediment's P retention capacity (Caraco et al., 1991).

While much of the work on sedimentary P cycling has focused on the behavior of soluble phosphate in relation to geochemical processes controlling inorganic P compounds, in particular phosphate sorption to clays and metal [Fe, manganese (Mn), aluminum (Al)] oxyhydroxides, there is mounting evidence that organic forms of P, and interactions between phosphate and humic substances, also play significant roles in controlling P exchanges between sediments and the overlying water column (Gerke, 2010; Li et al., 2017; Toor et al., 2006). Organic P compounds often represent a large proportion of the total P in aquatic systems (Giles et al., 2015; Monaghan & Ruttenburg, 1999; Read et al., 2014). Furthermore, a significant fraction (up to 60%) of organic P in sediments is potentially mobile and can therefore act as a long-term source of nutrient P to the water column (Cao et al., 2009; Rydin, 2000), hence, increasing the risk of eutrophication in lakes and reservoirs.

Stable complexes between humic substances and phosphate can be formed via bridging metal cations (Guardado et al., 2007; Riggle & Von Wandruszka, 2005). In addition to trivalent Fe and Al, a variety of divalent metals [calcium (Ca), magnesium (Mg), zinc (Zn), copper (Cu), manganese (Mn)] may bind phosphate anions to humic substances. Because the stability constants of phosphate-metal-humic complexes are of the same order of magnitude as those of the corresponding metal-humic complexes, humic-bound or organic-matter-complexed P is presumed to play a nonnegligible role in soil P dynamics (Guardado et al., 2007, 2008) and, by extension, possibly also in lake sediments of lakes receiving relatively large, with significant inputs of allochthonous organic matter, such as the Precambrian Shield lakes at the Experimental Lakes Area (ELA).

Lake 227 of the ELA presents a unique opportunity to analyze the response of sediment P speciation and accumulation rates to variations in trophic conditions (Schindler, 2009). This boreal lake has been artificially fertilized with P since 1969, causing the lake to transition from its original, oligotrophic state to a eutrophic state. The aims of this study were to (1) compare the effect of prefertilization and postfertilization on P speciation before and after 1969 in dated sediment cores collected from deep and shallow regions of the lake, using sequential chemical extractions, complemented by spectroscopic techniques [31P nuclear magnetic resonance (NMR), Mössbauer, and X-ray Adsorption Near-Edge Structure (XANES)], and (2) assess how the pools of P associated with sedimentary organic matter and Fe responded to the large shift in external P loading accompanying the long-term fertilization experiment.

2. Materials and Methods

2.1. Study Site and Sampling

Sediment cores were collected in the oxygenated epilimnion and the predominantly anoxic hypolimnion of Lake 227 (Figure 1). Lake 227 is part of the ELA in northwestern Ontario, Canada, which comprises 58 lakes with surface areas ranging from 1 to 84 ha. Since 1968, ELA has provided a unique natural laboratory to study in-lake physical, chemical, and biological processes during whole-ecosystem manipulation experiments, under conditions that are difficult, if not impossible, to reproduce in the laboratory (Malley & Mills, 1992; Schindler, 2009).

Lake 227 is a round headwater lake, 5 ha in area, with a maximum depth of 10 m in its center, a mean depth of 4 m, and a volume of 2.2×10^5 m^3 (Brunskill & Schindler, 1971; Figure 1). The lake's 29.4 ha watershed is characterized by siliceous lithology with bedrock ridges and thin tills, and a vegetation cover dominated by black spruce and jack pine forest (Schindler et al., 1987). A single stream leaves the lake, flowing over a steep bank into nearby Lake 305. Lake 227 is perched about 30–40 m above nearby lakes. The lake does not have significant subsurface (groundwater) outflow (Brunskill & Schindler, 1971). There are no inlet streams; the lake is fed via surface runoff, primarily during snowmelt and occasional heavy rainstorms.

In its natural, pre-1969 condition, Lake 227 was oligotrophic, with chlorophyll concentrations <2 μg L^{-1} and Secchi depths >4 m (Schindler, 1971). From 1969 to the present day, the lake has been fertilized without

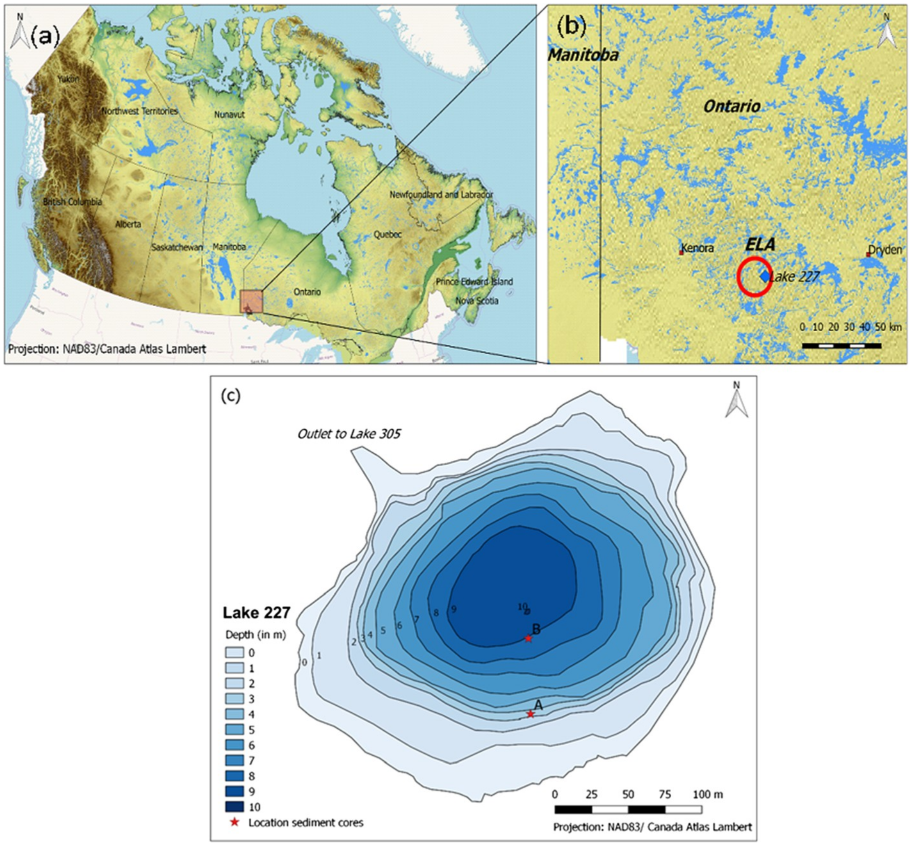

Figure 1. Location of the Experimental Lakes Area (ELA) in Ontario, Canada (a and b): The red circle indicates ELA, the blue diamond indicates the location of Lake 227. Bathymetric map and locations of the sediment cores (c) in the epilimnion (A) and hypolimnion (B).

interruption with P, receiving each year approximately 0.55 g P m^{-2} via 20–21 weekly additions during the ice-free season (Levine & Schindler, 1980; Schindler, 2009). From 1969 to 1990, the lake was also fertilized with nitrogen (N): from 1969 until 1974, N was added in a molar N:P ratio of 12:1; from 1974 to 1990, N additions were reduced to yield a N:P ratio of 4:1. Since 1990, Lake 227 has only been fertilized with P. Spring turnover is usually incomplete below 7 m, while fall turnover is seldom complete below 9 m. Anoxic conditions therefore prevail in the hypolimnion for most of the year. Stratification during the summer is well defined, with a 2–4 m thick epilimnion (Brunskill & Schindler, 1971).

Triplicate sediment cores were collected in October 2011 with a Glew gravity corer (diameter 7.5 cm) at water depths of 1 and 9 m, that is, in the epilimnion and hypolimnion, respectively. The sediment cores were sectioned into 1-cm intervals for the upper 5 cm, followed by 2-cm intervals down to 25 cm. Pore waters and solids were separated by centrifugation under N_2 atmosphere. Pore water pH, dissolved phosphate concentration (molybdate blue method, Murphy & Riley, 1962) and elemental composition (ICP-MS) were measured at the ELA field station immediately upon core sectioning. The pore water results are shown in Figure S1 (supporting information). The solid phase samples collected after centrifugation were freeze-dried for 48 hr. Total carbon (TC), total organic carbon (TOC) and total sulfur (TS) concentrations of the freeze-dried materials were analyzed on a LECO nutrient analyzer at the Agricultural and Food Laboratory, University of Guelph, Ontario. Whole-core sediment samples collected for the ^{31}P NMR analyses were transported on dry ice and processed wet to partially frozen immediately upon arrival. Note that the chemical extractions for P, Fe, and S were carried out on freeze-dried sediment core samples. While we cannot exclude possible artifacts associated with the freeze drying, the detection of amorphous and poorly crystalline Fe phases, as well as the reasonable depth distributions of the different species of P, Fe, and S, lead us to believe that no major artifacts were introduced that would invalidate the interpretation of the results (see sections 3 and 4).

2.2. Sediment Dating

Sediments were analyzed via gamma ray spectrometry for the radioisotopes ^{210}Pb (total), ^{214}Bi, ^{214}Pb, ^{137}Cs, ^{238}U, ^{232}Th, and ^{40}K, as described by Hall et al. (2012). Because Lake 227 was spiked with 2.1×10^{10} dpm of ^{226}Ra (added as $RaBr_2$) in August 1970 (Emerson & Hesslein, 1973), the amount of supported ^{210}Pb (=^{226}Ra) activity cannot be assumed to be constant throughout the core, as is often done (Appleby et al., 2001). The unsupported ^{210}Pb activity derived from atmospheric fallout was therefore calculated for each sediment interval individually. The resultant unsupported ^{210}Pb activity for each sediment interval and the integrated ^{210}Pb activities were then used to calculate the CRS (Constant Rate of ^{210}Pb Supply) and CF:CS (Constant Flux and Constant Sedimentation rate; linear model) ^{210}Pb age models as described by Appleby et al. (2001). The natural ^{226}Ra activities of the Lake 227 cores were estimated from the average of the bottom-most sediment interval from each core, where ^{226}Ra activity was observed to be near constant. The natural ^{226}Ra activities ($^{226}Ra_{nat}$) were 67.92 ± 1.83 and 25.74 ± 0.58 Bq kg^{-1} for the hypolimnion and epilimnion sediment cores, respectively.

2.3. Chemical Extractions: Phosphorus

The sediment core samples were extracted sequentially using a modified SEDEX protocol (for the flow diagram, see Figure S2, supporting information). The method is based on the SEDEX P sequential extraction method originally developed by Ruttenberg (1992) for marine sediments and adapted by Baldwin (1996) for freshwater sediments by adding a 1 M $NaHCO_3$ step to differentiate P associated with humic substances from P bound to reducible ferric iron (Fe) oxides. Note that this differs from the more common NaOH extraction (e.g., Gerke, 2010), which was used on separate sediment samples for the ^{31}P NMR analyses (see section 2.6). Li et al. (2015) also further showed that the citrate-bicarbonate-dithionate (CDB) extraction may mobilize P associated with colloidal Fe oxides-organic matter (OM) complexes. The P extraction scheme used here yielded the following operationally defined P fractions: easily exchangeable (P_{Ex}, 1 M $MgCl_2$), humic bound (P_{Hum}, 1 M $NaHCO_3$), Fe-oxide bound (P_{Fe}, CDB), $CaCO_3$ bound (P_{CFA}, 1 M acetate, pH 4), detrital apatite/other inorganic P (P_{Detr}, 1 M HCl), and organic P (P_{Org}, 1 M HCl after washing at 550°C). Hereafter, total inorganic P (TIP) refers to the sum of P released during the first five extraction steps and total P (TP) to the sum of TIP plus P_{Org}.

A 0.5-g aliquot of dry sediment was ground to a fine powder, then suspended in an acid-washed 50-ml centrifuge tube. All extractions were done in duplicate and at room temperature (22 ± 2°C). The solutions were continuously agitated during extraction (200 rpm). To collect the supernatant, the suspension was centrifuged for 15 min at 3,500 rpm, and the supernatant was carefully removed using syringe needles. Time between collection of the supernatant and analysis was kept as short as possible. For all extraction steps, except for the P_{Fe} and P_{Hum} extractions, the dissolved phosphate concentration was measured by flow injection analysis (Lachat Quickchem 8,500), with a precision better than 5%. The P_{Hum} extracts were measured on a UV-Vis spectrophotometer (ThermoEvolution 260) using the molybdate blue method (Murphy & Riley, 1962). The dissolved phosphate concentrations in the P_{Fe} extracts were determined by the isobutanol method of Watanabe and Olsen (1962), after reacting the solution with 1% *v*/v $FeCl_3$ to minimize the interference of citrate (Ruttenberg, 1992). Total dissolved P (TDP) concentrations were measured by inductively coupled plasma optical emission spectrometry (ICP-OES; Thermo Scientific iCAP 6,000) with an analytical precision <5%.

2.4. Chemical Extractions: Iron

Solid-phase Fe speciation was determined on sediment core samples following the sequential extraction protocol of Poulton and Canfield (2005). Note, however, that only the first six steps were carried out, yielding the following operationally defined Fe pools: loosely-sorbed (Fe_{Ex}, 1 M $MgCl_2$), carbonate-associated (Fe_{Carb}, 1 M sodium acetate), easily-reducible (Fe_{Ox1}, 1 M hydroxylamine-HCl solution), reducible (Fe_{Ox2}, 0.3 M sodium dithionate), magnetite (Fe_{Mag}, 0.2 M ammonium oxalate/0.17 M oxalic acid solution), and poorly reactive silicates (Fe_{PRS}, 12 N HCl). All extractions were done in duplicate with 0.1 g of dry sediment ground to a fine powder and suspended in an acid-washed 50-ml centrifuge tube. The supernatant was carefully removed and an extra washing step with deionized water was applied after each extraction step. Iron concentrations in the extracts were measured by ICP-OES. Analytical precision on the dissolved Fe measurements was <10%. After every 12 samples, a standard was run to correct for instrumental drift. Total reactive Fe

(TRFe) concentrations were calculated as the sum of Fe recovered in the six extractants using the Poulton and Canfield (2005) method, plus the concentration of Fe associated with Fe (II) monosulfides and pyrite derived from the sulfur (S) extractions (see section 2.5). Total Fe (TFe) concentrations were obtained by washing the sediments for 8 hr at 450°C and then dissolving in 6 M HCl under near boiling temperature for 24 hr.

2.5. Chemical Extractions: Sulfur

The following three solid-phase S pools were separated based on Burton et al. (2008): acid-volatile sulfide (S_{AVS}, 6 M HCl and 1 M ascorbic acid), which is usually assumed to represent Fe monosulfides, chromium-reducible S (S_{CR}, Cr (II) solution), which also extracts pyrite, and elemental S (S_{rhom}, dimethylformamide and Cr (II) solution). The extractions were performed in sealed Teflon reactors under continuous flow of argon (Ar) and agitation by a magnetic stirrer. All solutions were prepared with O_2-free water. The Cr (II) solution was obtained by reduction of a 2 M Cr $(III)Cl_3$ 0.5 N HCl solution by a Zn amalgam. Reaction time was 1 hr for each extraction step. Evolving H_2S was trapped by bubbling through a NaOH trap and quantified by colorimetry. Between steps, traps were filled with fresh NaOH and bubbled for 15 min with Ar, before proceeding to the next extraction step.

2.6. Chemical Extractions: Humic Fractions

The mobile humic acid (MHA) and the more recalcitrant calcium humate (CaHA) fractions were extracted from the sediments using the two-step procedure described by He et al. (2011) and subsequently examined by XANES as described in section 2.8. During the first step, MHA was extracted from the bulk sample with 0.25 M NaOH. The residue of this first extraction then underwent a 0.2 M HCl wash, followed by a second extraction with 0.25 M NaOH.

Specifically, 5 g of sediment from the 0–5 and 20–25 cm depth intervals of the epilimnion and hypolimnion cores were shaken in 50 ml of 0.25 M NaOH under N_2 for 20 hr. After centrifugation, the supernatant was decanted and acidified to pH 2 for precipitation of the MHA fraction. This extraction was repeated to ensure full recovery of the MHA fraction. The extracted sediment residue was repeatedly washed with 0.2 M HCl to bring the pH below 1. Subsequently, the sediment residue was washed with Milli-Q water until the pH returned to 2. The recalcitrant fraction (CaHA), which is assumed to be bound primarily to Ca, was then extracted following the same procedure as for MHA. Further treatment of both fractions involved washing with a 0.05 M KCl to 0.25 M KOH solution and then a 0.5% HCl-HF solution to remove mineral particles, and then rinsed repeatedly for 3 days against successively weaker HCl solutions and finally water. All fractions were dried by lyophilizing and stored until use.

2.7. ^{31}P NMR

Sediment P was further characterized using ^{31}P NMR spectroscopy on extracts from the 0–5 cm and 20–25 cm depth intervals of the epilimnion and hypolimnion cores. The P extractions were carried out using NaOH-EDTA extraction (Cade-Menun & Preston, 1996; Giles et al., 2015). Immediately upon arrival at the laboratory, 3 g of wet sediment were dissolved in 25 ml of extraction solution (0.25 M NaOH, 0.1 M EDTA) and mixed vigorously for 4 hr. Suspensions were then centrifuged at 3,500 rpm for ~20 min, and the supernatant solution was filtered through a 0.45 μm pore size filter. A 1-ml aliquot of the solution was diluted to 10 ml and afterward analyzed by ICP-OES for Al, Ca, Fe, Mg, Mn, and P. The remaining filtrate was frozen at −80°C and freeze dried (24–36 hr). Samples were redissolved and analyzed as previously described (Giles et al., 2015). Peaks were assigned to compounds or compound classes based on their chemical shifts relative to an external orthophosphoric acid standard, with the orthophosphate peak in all spectra standardized to 6 ppm; peak identifications were confirmed with spiking experiments (Cade-Menun, 2015; Giles et al., 2015). Peak areas were calculated by integration on spectra processed with 10 and 2 Hz line broadening using NUTS software (Acorn NMR, Livermore CA). Calculations for total orthophosphate monoesters and total orthophosphate diesters were corrected for degradation during extraction and analysis (Giles et al., 2015).

2.8. X-ray Absorption Spectroscopy: XANES

We used XANES spectroscopy to determine the oxidation state of Fe and delineate probable forms of P and Fe in bulk sediment samples, as well as in the MHA and CaHA humic fractions (see section 2.6). P and Fe K-edge spectra were collected at the Soft X-ray Microcharacterization Beamline (SXRMB), equipped with Si(111) and

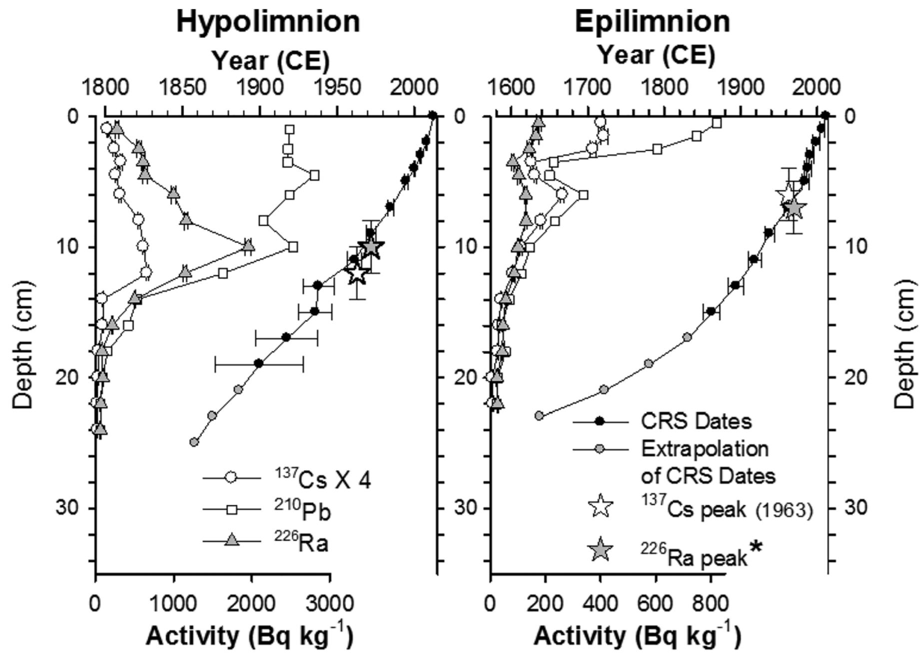

Figure 2. Hypolimnion and epilimnion sediment core activity profiles of ^{210}Pb, ^{226}Ra (* = mean of ^{214}Bi and ^{214}Pb) and ^{137}Cs, plus the CRS (CRS = Constant Rate of ^{210}Pb Supply) age-depth relationships. CE = Common Era.

InSb(111) double-crystal monochromators, at the Canadian Light Source (CLS), Saskatoon, Canada. The operating condition of the storage ring in CLS was 2.9 GeV with a maximum current of 250 mA. Powder P standards and sediment samples were thinly spread over a P-free, double-sided carbon tape. The sediment spectra were collected in partial fluorescence yield (FY) using a four-element Si-drift fluorescence detector, while spectra of P reference standards were measured in total electron yield (TEY), which is free of self-absorption effects. Multiple spectra (two for each standard and at least three for the sediment samples) were collected and averaged. Radiation damage was deemed negligible given the good reproducibility for each sample of repeated measurements on the same spot and repeated scans over different spots. The standards included in the analysis were ferrihydrite, goethite, ferric phosphate, apatite, vivianite, and phytic acid. XANES spectra were analyzed with the Athena software (Ravel & Newville, 2005). The energy scale was calibrated to 2,149 eV (E0) as the maximum energy of the first peak in the first derivative spectrum of $AlPO_4$ (Beauchemin et al., 2003). Linear regression fitting through the preedge region and normalized total K-edge intensity to one unit edge jump by defining the continuum regions (>50 eV above absorption edge) as the postedge region was used to background correct the spectra (Beauchemin et al., 2003).

2.9. ^{57}Fe Mössbauer Spectroscopy

Mössbauer spectra were obtained on bulk samples from two depth intervals (0–5 and 20–25 cm) in the epilimnion and hypolimnion cores. Sample preparation was identical to Peretyazhko et al. (2012). Spectra were acquired on a WissEl Elektronik instrument that included a closed-cycle cryostat SHI-850 (Janis Research), a CKW-21 He compressor unit (Sumitomo), and an Ar-Kr proportional counter detector (LND Inc.). A ^{57}Co/Rh source (50-m Ci to 75-m Ci, initial strength) was used to generate the gamma radiation. The transmitted counts were stored in a multichannel scalar (MCS) as a function of energy (transducer velocity) using a 1,024-channel analyzer. The raw data were folded to 512 channels to provide a flat background and a zero-velocity position corresponding to the center shift (CS) of a metal Fe foil at room temperature. Calibration spectra were obtained with a 7-µm-thick Fe foil placed in the same position as the samples to minimize any geometry errors. The data were modeled with the Recoil software using a Voigt-based structural fitting routine (Rancourt & Ping, 1991). Spectra were obtained at room temperature (RT), 140 K, 77 K, and 8.8 K and compared to reported Mössbauer spectral parameters of pure Fe phases. The selected measurement temperatures are optimal for characterizing natural Fe-oxide assemblages (Peretyazhko et al., 2012).

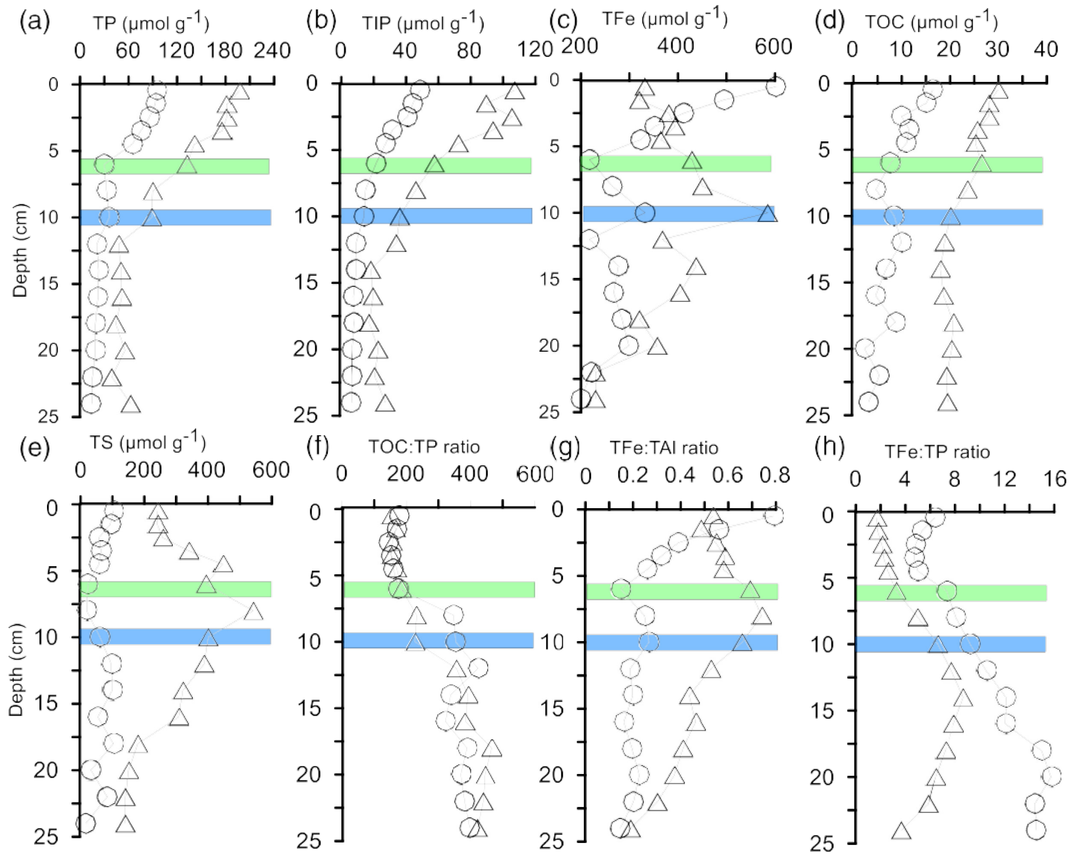

Figure 3. Solid-phase depth distributions of (a) total P (TP), (b) total inorganic P (TIP), (c) total Fe (TFe), (d) total organic carbon (TOC), (e) total sulfur (TS), (f) molar TOC:TP ratio, (g) molar TFe:TAl ratio, and (h) molar TFe:TP ratio, in the hypolimnion (Δ) and epilimnion (o) sediments. Fertilization initiation is denoted by (green horizontal bar) in the epilimnion (~6 cm) and (blue horizontal bar) in the hypolimnion (~10 cm) sediment profiles.

3. Results

3.1. Sediment Properties, Mass Accumulation Rates, and Elemental Compositions

Sediments of the hypolimnion cores were dark colored and consisted of fine-grained, organic-rich flocculent material. In contrast, sediments of the epilimnion cores were coarser and of lighter color; and quartz grains could easily be detected. Porosity in the upper 5 cm of all cores exceeded 90%. The ^{210}Pb-based age CRS models implied a higher whole-core linear sedimentation rate at the hypolimnion location compared to the epilimnion location (Figure 2). The ^{137}Cs and ^{226}Ra peak activities were consistent with the ^{210}Pb dating. Further note that, while the ^{226}Ra activity profiles showed evidence for both downward and upward movement of ^{226}Ra, the peak in activity due to the experimental addition in 1970 was preserved.

Based on the dating results and the compositional data presented below, the start of fertilization of Lake 227 coincided with depths of 6 and 10 cm in the epilimnion and the hypolimnion cores, respectively. Using these cutoff depths, the average pre-1969 sediment mass accumulation rates at the two locations were around 0.007 g cm^{-2} yr^{-1} for both the epilimnion and hypolimnion, while the post-1969 rates were higher, with 0.012 and 0.008 g cm^{-2} yr^{-1} for the epilimnion and hypolimnion, respectively (Figure S3). Note that while after 1969 the mass accumulation rate of the epilimnion is higher than for the hypolimnion, the linear sedimentation rate is lower (Figure 2). This is due to the higher mineral fraction and, therefore, higher dry density of the sediments deposited in the lake's littoral zone. The sediment surface area overlain by the epilimnion is around 24,000 m^2, which is almost on par with that covered by the hypolimnion at 26,000 m^2. Thus, the post-1969 total mass accumulation of sediment in Lake 227 is estimated at around 6.4 tons per year.

The TOC abundance in the hypolimnion (9 m water depth) sediments (27–36%) systematically exceeded that in the epilimnion (1-m water depth) sediments (6–19%; Figure 3). In both cores, the highest TOC concentrations, 19% and 36%, were observed in the 0–1-cm depth intervals of the epilimnion and hypolimnion, respectively. At both locations, TOC concentrations decreased with depth in the upper parts of the cores. In the epilimnion cores TOC stabilized at 8 ± 3% below 6 cm; in the hypolimnion cores, TOC concentrations below 12 cm remained close to 25 ± 3%. The hypolimnetic sediments also exhibited systematically higher TS concentrations than the epilimnetic sediments (Figure 3). In the epilimnion sediments, TS concentrations decreased from a maximum of 103 μmol g^{-1} at the SWI to a minimum of 16 μmol g^{-1} at 23–25 cm. In contrast, the hypolimnion profiles showed an increase in TS from 240 μmol g^{-1} at 0–1 cm to a maximum of 542 μmol g^{-1} at 7–9 cm, followed by a progressive decline to a minimum of 141 μmol g^{-1} at 23–25 cm.

The TP concentration profiles changed markedly with the onset of artificial fertilization, with concentrations increasing by factors of 3–4 at both coring locations (Figure 3). In the epilimnion core, the TP concentration was highest in the topmost centimeter (95 μmol g^{-1}) and dropped to values ≤20 μmol g^{-1} at depths below 6 cm. The hypolimnion sediments had consistently greater TP concentrations compared to the epilimnion location: TP decreased from a core-top (0–1 cm) maximum of 197 to about 40 μmol g^{-1} at 12 cm, below which the TP concentrations remained relatively constant. The depth trends of total inorganic P (TIP) roughly followed those of TP, with TIP concentrations approximately half those of TP.

The TFe depth profiles were quite different between the epilimnion and hypolimnion cores (Figure 3). Sediment TFe concentrations in the epilimnion sediments generally decreased with depth, from a maximum of 602 μmol g^{-1} (0–1 cm) to a minimum of 200 μmol g^{-1} (23–25 cm). In the hypolimnion sediments, the TFe concentrations first increased with depth, from 332 μmol g^{-1} (0–1 cm) to 585 μmol g^{-1} (9–11 cm), and then decreased down to 230 μmol g^{-1} (23–25 cm). The subsurface TFe maximum in the hypolimnion sediments was not unlike that observed for TS. Total aluminum (TAl) in the epilimnion sediments generally showed an inverse trend to that of TFe and, as a result, the TFe:TAl ratio in the epilimnion sediments showed a relative enrichment in Fe from the 5–6-cm depth interval up to the SWI, while the deeper sediment (>7 cm) was characterized by fairly constant molar TFe:TAl ratios, on the order of 0.15 (Figure 3). By contrast, the hypolimnion core TFe:TAl ratio showed a middepth maximum of 0.74 in the 7–9-cm depth interval.

One of the most diagnostic sediment signatures of the trophic transition of Lake 227 was the clear depth separation of the molar TOC:TP ratios at both locations, with fairly constant but relatively low values (around 170) in the upper parts of the sediments, and relatively constant but relatively high values (around 400) in the lower parts (Figure 3). The key difference between the two locations was the depth at which the transition was observed: around 6 cm for the epilimnion and 10 cm for the hypolimnion.

By combining the sediment mass accumulation rates with the sediment concentration data, element mass accumulation rates were calculated (Figure 4). For TOC, TP, and TFe, the relative increases in concentration in the epilimnion sediments after the start of fertilization were amplified by the significantly higher post-1969 sediment accumulation rates (Figure S3, supporting information). This effect was less pronounced for the hypolimnion sediments, because of the more limited post-1969 increase in the sediment accumulation rate. Interestingly, although the post-1969 hypolimnion sediments had lower TFe concentrations than their pre-1969 counterparts, the TFe accumulation rates remained fairly similar, implying that the lower post-1969 TFe concentrations primarily reflect the dilution by the higher accumulation of organic matter in the sediments.

3.2. Chemical Extractions: P Pools

At both coring locations, P released during the final step of the sequential extraction protocol (P_{Org}) represented between 45% and 65% of TP at all depths sampled (Figure 5, see also Figure S4, supporting information). This step is assumed to release the less-soluble P-containing organic compounds not extracted in earlier steps, especially during extraction by $NaHCO_3$ (Baldwin, 1996). The relative abundances of the acetate- (P_{CFA}) plus HCl-extractable P fractions (P_{Detr}) were distinctly lower (2–12%) in the upper parts of the cores, compared to the bottom parts (12–39%). For the hypolimnion, the up-core drop in the combined proportion of P_{Detr} plus P_{CFA} was compensated by the increase in the percentage of $NaHCO_3$-extractable P (P_{Hum}). By contrast, for the epilimnion, the lower relative proportion of P_{CFA} plus P_{Detr} in the upper portion of the core was compensated by the combined increases in the fractions of P_{Hum} and P_{Fe} (Figure 5).

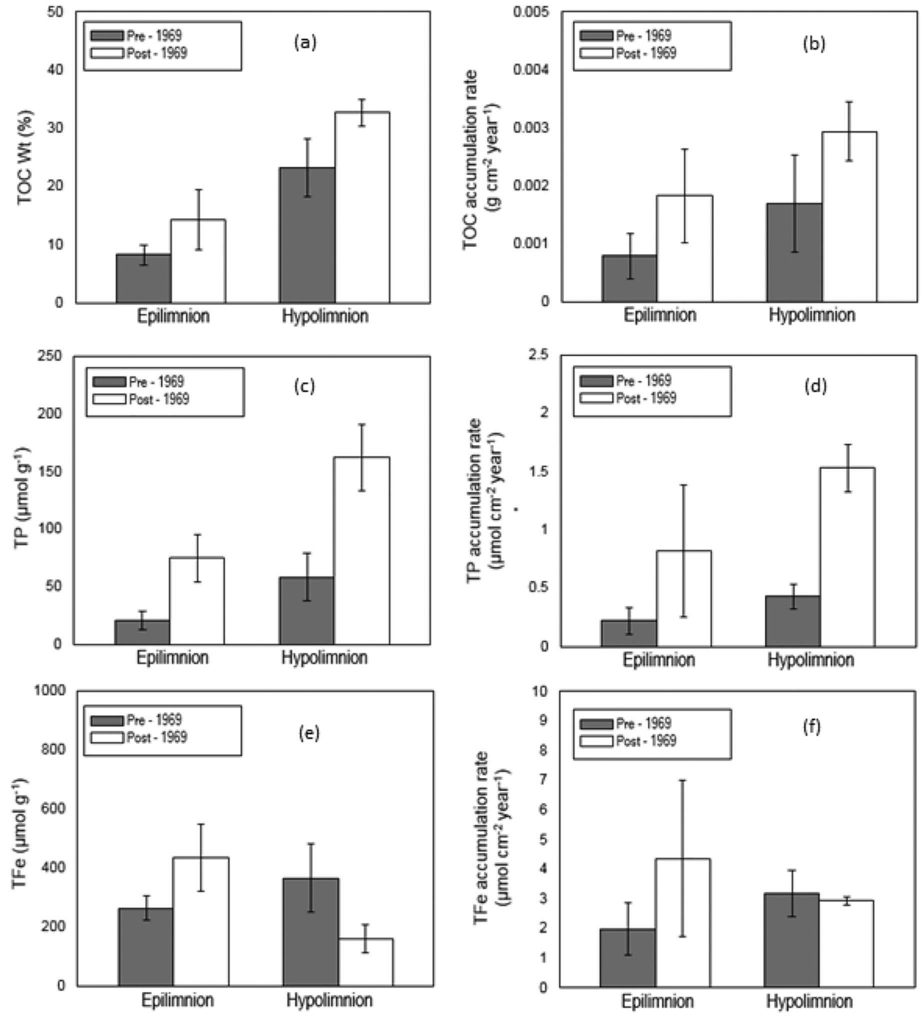

Figure 4. Total elemental concentrations and accumulation rates for TOC (a and b), TP (c and d), and TFe (e and f) in the epilimnion and hypolimnion sediment cores, for prefertilization and postfertilization (1969) conditions. The panels show mean values and standard deviations for the individual sediment intervals collected in each core.

In the upper 5 cm of both sediments, over 70% of TP was extracted in the second (P_{Hum}) plus last (P_{Org}) sequential steps, implying that P in the post-1969 sediments was predominantly associated with organic matter (Figures 5 and S4). The largest change in P fractions across the transition in lake trophic state, however, was the post-1969 increase in the P_{Hum} fraction. In the 0–5-cm depth intervals, P_{Hum} made up 30–40% of TP in the hypolimnion core, compared to about 20% in the epilimnion core. In the pre-1969 sections of the cores, P_{Hum} made up about 13% and 10% of TP at the hypolimnion and epilimnion locations, respectively (Figures 5 and S4).

3.3. Chemical Extractions: Fe Pools

The Fe_{Ox1} plus Fe_{Ox2} pools dominated reactive Fe throughout the epilimnion sediment profiles (Figure 5, see also Figure S5, supporting information). Together, Fe_{Ox1} and Fe_{Ox2} made up 77–84% of reactive Fe in the upper 6 cm of the epilimnion sediments. Not unexpectedly, the abundance of the most reactive fraction, Fe_{Ox1}, was highest in the 0–1-cm depth interval, where it represented nearly 60% of total reactive Fe. Below 7 cm, the fraction of Fe_{Ox1} dropped to 16–28% of total reactive Fe. Loosely-sorbed Fe only constituted a few percent of total reactive Fe, even close to the SWI, while the sulfur extractions did not detect pyrite in the epilimnion sediments (see also section 3.4).

10.1029/2020JG005713

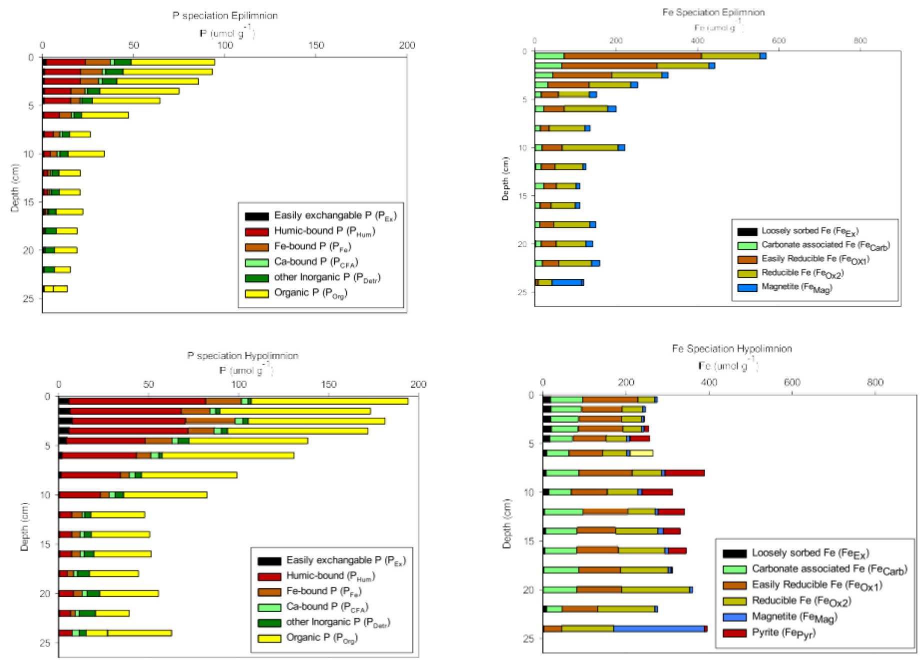

Figure 5. (left column) Phosphorus (P) and (right column) iron (Fe) speciation in the (top row) epilimnion and (bottom row) hypolimnion sediment cores in units of μmol g^{-1} (dry weight). The data shown are from the sequential extractions described in sections 2.3 and 2.4.

The sediment Fe composition in the lower portions of the epilimnion and hypolimnion cores (≥15 cm) was quite similar, with Fe_{Carb}, Fe_{Ox1} plus Fe_{Ox2} comprising about 90% of total reactive Fe. In the more recently deposited sediments, the distribution of reactive Fe among the various fractions differed, however. In particular, Fe_{Ex} and Fe_{Carb} played relatively larger roles in the core top hypolimnion sediments. Furthermore, in the 3–17-cm depth interval of the hypolimnion sediments the presence of pyrite was inferred, with a maximum contribution to total reactive Fe of 24% in the 7–8 cm interval. Nonetheless, Fe_{Ox1} and Fe_{Ox2} still represented 60–67% of total reactive Fe in the upper 7 cm, with a slight increasing core-up trend in the abundance of Fe_{Ox1} versus that of Fe_{Ox2}. There were strong positive correlations between the Fe and P concentrations mobilized during the $NaHCO_3$ extractions from both the epilimnion and hypolimnion (Figure S6, supporting information). These extractions release soluble organic matter from the sediments, including humic compounds (Baldwin, 1996).

3.4. Chemical Extractions: S Pools

The hypolimnion sediments exhibited a distinct TS enrichment in the middepth region, between 3 and 18 cm (Figure 3), which coincided with the inferred presence of AVS, elemental S and, in particular, pyrite-S (Figure S7, supporting information). The extractions did not detect any AVS, pyrite-S or elemental S above 3 cm and below 18 cm. The maximum TS concentration in the 8–10-cm depth interval also coincided with the highest TFe concentrations and Fe/Al ratios measured in the hypolimnion sediment samples (Figure 3). In the same depth interval, the concentrations of pyrite-S, AVS, and elemental S reached their maximum values of 192, 17, and 86 μmol g^{-1}, respectively. Note that the pyrite-Fe concentrations were calculated from the corresponding pyrite-S concentrations, assuming a molar 1:2 ratio.

The chemical extractions did not detect AVS, pyrite-S, or elemental S in any of the epilimnion sediment samples. The TS concentrations measured in the epilimnion sediments further correlated positively with the TOC concentrations (Figure S8, supporting information). The TS and TOC concentrations above 3 cm and below 18 cm in the hypolimnion sediments, that is, the depth intervals where no inorganic S was observed, coincided with the trend defined by the epilimnion sediments, with a molar TOC:TS ratio of approximately 100. The hypolimnion data from the intermediate 3–18-cm depth interval where inorganic S is enriched departed from this trend and yielded TOC:TS values that were distinctly lower than 100.

Table 1
Phosphorus Forms Determined by Phosphorus-31 Nuclear Magnetic Resonance Spectroscopy in NaOH-EDTA Extracts From the Epilimnium (Epi) and Hypolimnium (Hypo) Sediments

	Inorganic P (P_i)				Organic P (P_o)					
	NE-extracted P[a] (%)	Orth[b]	Pyro	Poly	Phon	Total mono	Total Di	M:D ratio	Total P_i	Total P_o
Depth (cm)		% Extracted P							% Extracted P	
Epi 0–5 cm	28.2	48.7	11.6	3.7	1.4	21.3	13.3	1.6	64.0	36.0
Hypo 0–5 cm	13.3	56.4	0.6	4.3	0.7	22.4	15.6	1.4	61.3	38.7
Epi 20–25 cm	23.6	43.1	0.0	1.4	1.4	39.8	14.3	2.8	44.5	55.5
Hypo 20–25 cm	13.9	53.1	0.1	0.6	1.4	24.9	19.9	1.3	53.8	46.2

Note. The 0–5 cm depth intervals correspond to sediments deposited after fertilization was started, the 20–25 cm depth intervals precede fertilization.
[a]The percentage of total chemical extracted P that was extracted by NaOH-EDTA (NE). [b]orthoP, orthophosphate; pyro, pyrophosphate; poly, poly-phosphate; phon, phosphonates; total mono, total orthophosphate monoesters, corrected for degradation artifacts; total di, total orthophosphate diesters, corrected for degradation artifacts; M:D, the ratio of orthophosphate monoesters to diesters; total pi, total inorganic phosphate; Total Po, total organic phosphate.

These low TOC:TS values are thus diagnostic of Fe sulfide mineral precipitation and pyritization in the hypolimnion sediments under the eutrophic, post-1969 conditions.

3.5. ^{31}P NMR

The ^{31}P NMR spectra of the NaOH/EDTA extracts showed marked differences between the two locations, and between oligotrophic (pre-1969) and eutrophic (post-1969) lake conditions (Table 1 and Figure S9, supporting information), although, as generally observed in lake sediments (e.g., Ahlgren et al., 2005; Giles et al., 2015), orthophosphate was the dominant form of P in all the extracts. Generally, the epilimnion sediment samples yielded the spectra with the best resolution, compared to those from the hypolimnion. This was especially true for the epilimnion spectrum from the 20–25-cm interval (Figure S9). Lower resolution of the other spectra may be due to increased viscosity from organic matter and increased line-broadening from Fe, consistent with the higher TOC, TFe, and P_{Hum} concentratrions. We tested sample dilution to decrease viscosity, which improved the resolution somewhat.

In the epilimnion sample from 20–25 cm, we clearly identified a number of different inositol hexaphosphate stereoisomers, similar to what was reported by Giles et al. (2015). However, due to uncertainties in identifying the same peaks for the hypolimnion samples, quantitative estimates were only made for total orthophosphate monoesters and total orthophosphate diesters, after correction for diester degradation (Table 1). For both the hypolimnion and epilimnion, the relative contributions to NaOH/EDTA extracted P of inorganic P (the sum of orthophosphate, pyrophosphate, and polyphosphate) were greater in the 0–5 cm interval (64% and 61% for epilimnion and hypolimnion, respectively) than in the 20–25 cm interval (44.5% and 54%, respectively). Orthophosphate monoesters consistently made up a higher fraction of P extracted by NaOH/EDTA in the deeper intervals than the shallower intervals. Monoesters were also systematically more abundant than diesters in all samples analyzed.

3.6. XANES

Both Fe and P K-edge XANES spectra were collected on Fe and P reference compounds, bulk sediments from the epilimnion and hyplimnion cores (0–5 and 15–20 cm), and the corresponding humic extracts MHA and CaHA (Figure 6). The Fe K-edge results indicated that Fe (III), rather than Fe (II), dominated Fe speciation in the bulk sediments of both cores and at both depth intervals, consistent with the chemical extraction results (Figures 5 and S5). The Fe K-edge spectra of the MHA and CaHA extracts were very similar to those obtained for the bulk sediments, suggesting that binding to humic compounds contributed to the stabilization of ferric Fe. The P K-edge spectra in all bulk and humic extract samples most closely resembled that of the phytic acid standard (Figure S10, supporting information). Hence, according to the XANES spectra, most sediment P appeared to be bound in organic compounds, as also implied by the ^{31}P NMR results.

3.7. ^{57}Fe Mössbauer Spectroscopy

The results of the Mössbauer spectroscopy derived bulk sediment Fe speciation are summarized in Table 2; observed and fitted Mössbauer spectra at 8.8 K are shown in Figure 7. The spectra of the 0–5-cm and 20–25-

10.1029/2020JG005713

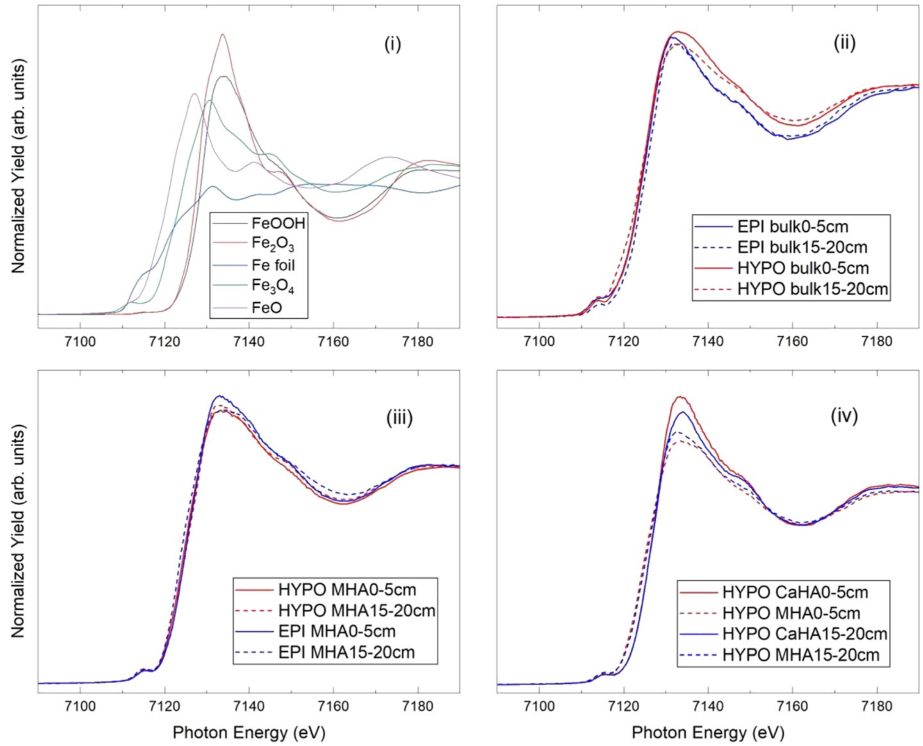

Figure 6. Iron K-edge XANES spectra of (i) reference standards, and for (ii) bulk sediment, (iii) mobile humic extracts (MHA), and (iv) mobile (MHA) and recalcitrant humic extracts (CaMA) of the 0–5 cm and 15–20 cm depth intervals of the epilimnion and hypolimnion cores.

cm intervals of the epilimnion core were very similar, hence only the 0–5-cm results are presented. The dominant room temperature (RT) ferric doublet (about 90% of the spectral signal) transformed into multiple sextets at 8.8 K (Figure 7). The extent of transformation, however, was gradual and increased with decreasing temperature, indicating that the RT Fe (III) doublet was a composite of several Fe (III) pools with variable doublet-to-sextet transition temperatures. For instance, the Mössbauer spectral parameters of the 140 and 77 K sextets (~23% spectral area) are within the range of small-particle goethite (Figure S11, see Bhattacharyya et al., 2018). The RT spectral features, also implied that large-particle goethite, hematite, and magnetite, were not constituents of the sediments.

Modeling of the 8.8 K epilimnion spectrum yielded one fraction of the total Fe pool under the form of small-particle goethite (A and B in Table 2), and one fraction consisting of ferrihydrite-like mineral species (C and D in Table 2). The ferrihydrite-like mineral phases were likely associated with organic matter (OM) (Chen et al., 2015), silicon (Zhao et al., 1996), and, possibly, phosphate (Borch et al., 2010), based on the broad hyperfine field distributions. In reality, species C and D represent a continuum of ferrihydrite-like phases with a distribution of crystallinity and variable amounts of sorbed OM and phosphate that increase toward the D end-member. The species labeled E in Table 2 was tentatively identified as structural Fe (III) in phyllosilicates, although it could also include contributions from high spin Fe (III) in apatite (Shao et al., 2014). The high-spin HS Fe (II) probably comprised phyllosilicate and apatite Fe (II).

Ferric iron oxides (goethite, hematite, and magnetite), whether as large particles or nanoparticles, were not detected in the 0–5-cm hypolimnion sample (Table 2), based on the absence of well-defined sextets in the RT, 140 and 77 K Mössbauer spectra (Figure S11). A small fraction of small-particle goethite, however, was present in the 20–25-cm depth interval, based on the presence of a minor sextet feature (B′) in the 77 K spectrum. A sizeable fraction of total Fe in both hypolimnion depth intervals was composed of ferrihydrite-like species (C′ and D′, Figure 7) but with somewhat different Mössbauer parameters than species C and D in the epilimnion sediments, possibly because of differences in the Fe:OM or Fe:P ratios. More importantly, Mössbauer spectral features indicative of pyrite (species G) (Shao et al., 2014) and Fe (III)-OM-like

Table 2

Contributions of Different Fe Pools That Explain the Fits to the ^{57}Fe Mössbauer Spectra at 8.8 K Shown in Figure 8 for Bulk Sediments of the Epilimnion (0–5 cm Depth Interval) and Hypolimnion (0–5 cm and 20–25 cm Depth Intervals) of Lake 227

Fe species	% total Fe	Description
Epilimnion (0–5 cm)		
HS Fe (II)[a]	7	Phyllosilicate Fe (II), apatite Fe (II)
HS Fe (III)-A,B	23	A-Small particle goethite/magnetite (8%)
		B-Small-particle goethite with/without coatings P & OM (15%)
HS Fe (III)-C	21	C-Ferrihydrite phase with coatings P & OM
HS Fe (III)-D	36	D-OM-ferrihydrite coprecipitate
HS Fe (III)-E	14	E-Phyllosilicate Fe (III), Apatite Fe (III)
Hypolimnion (0–5 cm)		
HS Fe (II)	<3%	Phyllosilicate Fe (II), apatite Fe (II)—based on RT spectrum
HS Fe (III)-A	0	A-Small particle goethite/magnetite
HS Fe (III)-B′	0	B-Small-particle goethite with coatings P & OM
HS Fe (III)-C′	16	C-Ferrihydrite with coatings P & OM
HS Fe (III)-D′	45	D-OM-ferrihydrite coprecipitate (different from Epilimnion)
HS Fe (III)-E	0	E-Phyllosilicate Fe (III), apatite Fe (III)—small amounts likely
HS Fe (III)-F	15	F-OM-Fe (III) complex
LS Fe (II)-G[b]	24	G-Pyrite
Hypolimnion (20–25 cm)		
HS Fe (II)	<3%	Phyllosilicate Fe (II), apatite Fe (II)—based on RT spectrum
HS Fe (III)-A	0	A-Small particle goethite
HS Fe (III)-B′	8	B-Small-particle goethite with coatings P & OM—based on 77 K
HS Fe (III)-C′	29	C-Ferrihydrite with coatings P & OM (B′ & C′ are shown as a sextet in figure)
HS Fe (III)-D′	47	D-OM-ferrihydrite coprecipitate (different from Epilimnion)
HS Fe (III)-E	0	E-Phyllosilicate Fe (III), Apatite Fe (II)—small amounts likely
HS Fe (III)-F	4	F-OM-Fe (III) complex
LS Fe (II)-G[b]	12	G-Pyrite

[a]High-spin Fe (II). [b]Low-spin Fe (II) (e.g., pyrite).

complexes (species F) (Jung et al., 2012) were found at both depth intervals of the hypolimnion, but not in the epilimnion sediments. The relative amounts of ferrihydrite and pyrite (G), however, were different in the 0–5-cm (higher pyrite) and (higher ferrihydrite) 20–25-cm hypolimnion sediments.

3.8. P Budget: Prefertilization and Postfertilization

Average TP budgets before and after the onset of the artificial fertilization are compared in Figure 8. The annual TP surface runoff to Lake 227 was estimated using the range of TP export coefficients for similar Precambrian shield lake catchments reported in the literature, including for nearby Lake 239 (0.7–10 mg P m^{-2} yr^{-1}, Dillon & Rigler, 1975; Dillon & Molot, 1997; Parker et al., 2009). Combined with Lake 227's catchment surface area (29.4 ha) this yielded an average runoff of 1.6 kg P yr^{-1}, with a range of 0.2–3 kg P yr^{-1}. Based on our estimated pre-1969 TP burial rates of 1.6 and 3.1 kg P yr^{-1} for epilimnion and hypolimnion sediments, respectively, a total prefertilization sediment mass accumulation of 4.7 kg P yr^{-1} was estimated (range: 3.5–5.5 kg P yr^{-1}). The outflow flux of TP from the lake was calculated assuming an average flushing time of the lake of 4 years (range: 1.6 to 6.8 years for the period 1970–1992, ELA database) and an average prefertilization TP concentration in the outflow of 10 μg L^{-1} (Schindler, 1971). The prefertilization outflow flux was therefore 0.6 kg P yr^{-1} (range: 0.4–1.1 kg P yr^{-1}).

An additional natural source of TP to the lake is atmospheric deposition (Meinikmann et al., 2015). The atmospheric TP deposition contribution was calculated by assuming that the prefertilization TP budget was at steady state. The resulting atmospheric deposition of 3.7 kg P yr^{-1} (range 1.2–5 kg yr^{-1}) corresponds to a surface-normalized atmospheric deposition rate of 74 mg P m^{-2} yr^{-1}, which is comparable in magnitude to values reported for other pristine lakes in Canada and globally (Dillon & Molot, 1997; Shaw

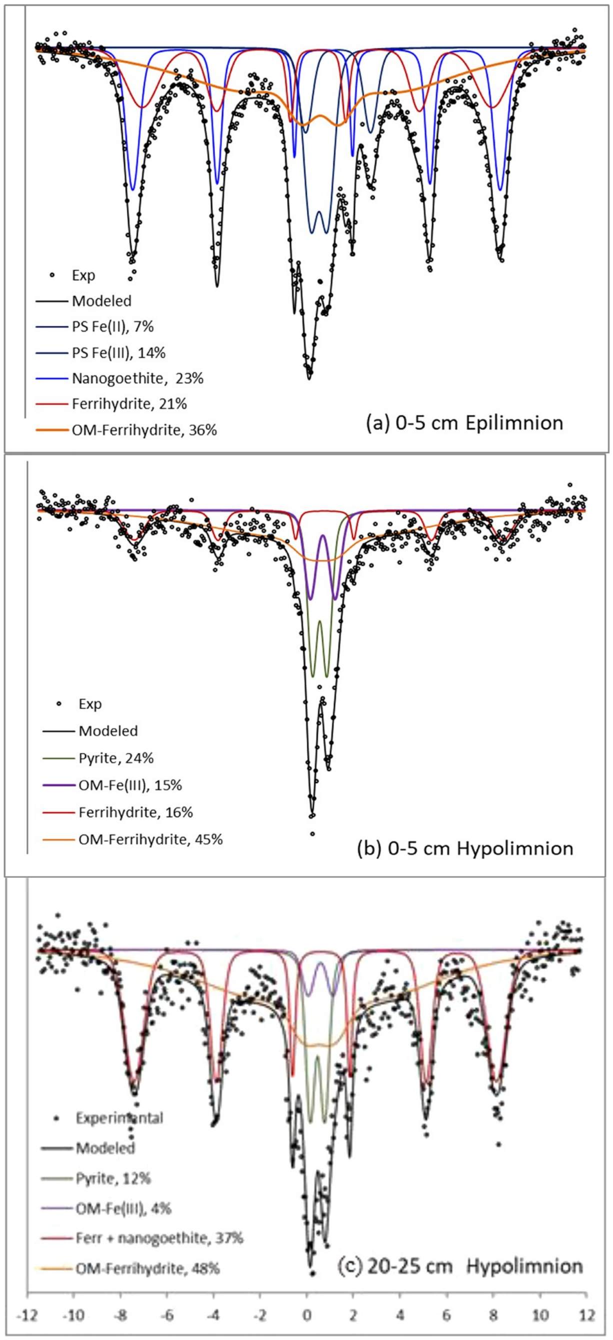

Figure 7. Fitted ^{57}Fe Mössbauer spectra at 8.8 K of (a) 0–5 cm depth interval of epilimnion sediment (the 0–5 cm and 20–25 cm epilimnion depth interval spectra are similar), (b) 0–5 cm, and (c) 20–25 cm depth intervals of hypolimnion sediment. The black solid lines are the total calculated fits through the discrete data points (black dots), the other lines show the contributions of individual Fe species.

et al., 1989; Tipping et al., 2014). For ELA's Lake 373, atmospheric TP deposition associated with pollen was reported to be 37 mg P m^{-2} yr^{-1} (Graham et al., 2006). If this value is representative for Lake 227, then about half of atmospheric TP deposition onto Lake 227 could be supplied by pollen. According to the above calculations, atmospheric deposition represented about 70% of the pre-fertilization TP inputs to Lake 227, which is close to the 72–73% estimated for ELA's headwater Lake 373 during 1991–1992 (Campbell, 1994).

During the post-1969 period, on average 24 kg P yr^{-1} was added annually to Lake 227 (range: 19.8–31.9 kg P yr^{-1}, Schindler et al., 2008), which is very close to the average epilimnion plus hypolimnion TP mass accumulation rate in post-1969 sediments determined in the present study (26.8 kg P yr^{-1}, Figure 8). That is, most of the artificially supplied P was balanced by increased sedimentary P burial. Assuming that the natural supply of TP via surface runoff and atmospheric deposition remained the same before and after artificial fertilization was initiated (5.3 kg P yr^{-1}), and assuming a (near-) steady state post-1969 TP budget, the outflow TP flux should be equal to 2.5 kg P yr^{-1} (range: 2.0–3.0 kg P yr^{-1}). For an average water renewal time of 4 years, the outflow flux translates in an average outflow TP concentration of 45 µgP yr^{-1}, a value closely matching the average post-1969 TP concentration measured in the epilimnion of 42 µgP yr^{-1} (Schindler et al., 2008).

4. Discussion

4.1. Trophic Transition: Sediment, TOC, and Fe Accumulation

The epilimnion and hypolimnion sediments display clear signatures of the transition in lake trophic state of Lake 227 initiated in 1969 with the artificial additions of P. Before the artificial fertilization, the mean sediment mass accumulation rates were about the same in the epilimnion and hypolimnion. In the epilimnion, the average sediment mass accumulation rate during the fertilization period (0.012 g cm^{-2} yr^{-1}) was nearly double that in the prefertilization period (0.007 g cm^{-2} yr^{-1}; Figure S3). The sediment accumulation rate in the hypolimnion showed a relatively smaller increase during fertilization. As indicated by the simultaneous increases in TOC concentrations (Figure 4), the enhanced sediment accumulation rates can be explained by increased deposition and preservation of algal detritus produced in-lake. In particular, the average TOC accumulation rate of the epilimnion more than doubled after artificial fertilization started, reaching a value close to 0.002 g C cm^{-2} yr^{-1}. Nonetheless, even during the fertilization period, more TOC accumulated per unit sediment surface in the deeper sediments of the hypolimnion.

The concentrations and accumulation rates of TFe show different responses to the artificial fertilization than TOC. In the epilimnion, the average sediment TFe accumulation rate more than doubled after 1969 while there was little change, or even a slight decrease, in the hypolimnion (Figure 4). In particular, a large increase in easily reducible ferric Fe (Fe_{Ox1}) was observed for the epilimnion sediments (Figures 5 and S5), while the reducible ferric Fe pool (Fe_{Ox1} + Fe_{Ox2}) in the hypolimnion sediments actually shrank (Figure S5). That is, the shift from oligotrophic to eutrophic conditions caused a redistribution of Fe accumulation in the lake: whereas per unit sediment surface area more TFe accumulated in the hypolimnion before fertilization than in the epilimnion, the opposite was observed during the fertilization period. The likely reason is that the increased reducing conditions in the post-1969 bottom waters of the hypolimnion were less conducive to

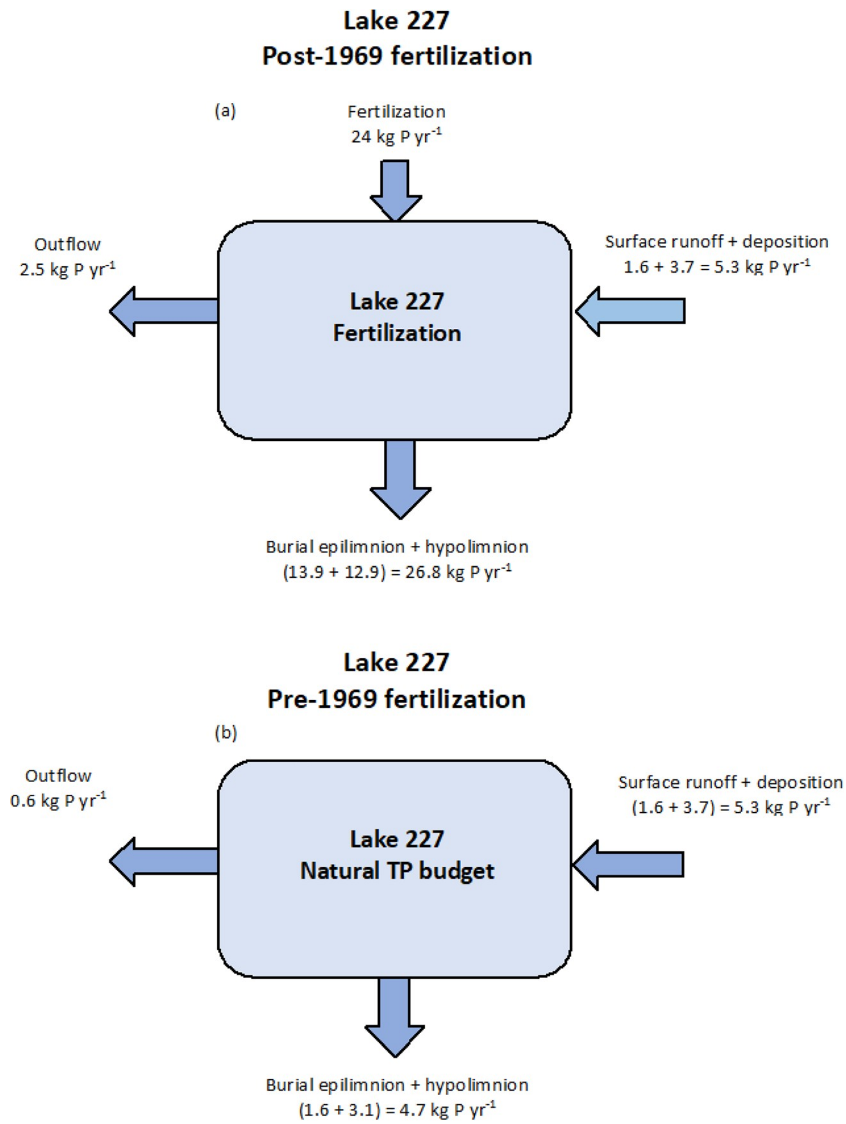

Figure 8. Total phosphorus (TP) budgets for Lake 227 during (a) the fertilization period (2011–1969) and (b) before fertilization started, that is, from the bottom of the cores up to the 1969 time line.

the formation and preservation of Fe (III) oxides. Remobilization of soluble Fe to the water column and lateral mixing would then have transferred Fe toward the lake's littoral zone (Schroth et al., 2015; Welch & Cooke, 2005), where the oxygenated bottom waters promoted the accumulation of Fe (III) oxides in the sediments (Kleeberg et al., 2013). Further research will be needed to fully delineate how nearshore-offshore chemical exchanges are recorded by the sediments of the hypolimnion and epilimnion.

In lakes with elevated organic matter terrestrial organic matter inputs one process that may help protect deposited organic matter from degradation in the epilimnion sediments is the strong binding of organic compounds to reactive Fe (III) mineral phases, that is, the Fe_{Ox1} pool (Barber et al., 2017; Lalonde et al., 2012). This hypothesis is supported by both the large post-1969 increase in the Fe_{Ox1} pool (Figure 5), and the large fraction of Fe (III) associated with OM in the epilimnion sediments inferred from the Mössbauer results (57% of TFe according to Table 2). In contrast, there was no significant increase in the Fe_{Ox1} pool in the hypolimnion sediments across the trophic transition (Figure 5), implying little change in the capacity to form Fe (III)-OM complexes. In addition, in-lake produced (autochthonous) organic matter is readily decomposed by heterotrophic microbes and, thus, less prone to accumulation in sediments in the absence of stabilization by mineral phases (Burdige, 2007; Ho & Meyers, 1994; Sobek et al., 2006).

4.2. Trophic Transition: P Accumulation

Lake eutrophication often coincides with increased sedimentary accumulation of TP (O'Connell et al., 2015). This is also the case for Lake 227: From oligotrophic to eutrophic conditions, the sediment TP concentrations and accumulation rates increased more than threefold for both epilimnion and hypolimnion (Figure 4). The relative increases in TP far exceeded those of TOC, hence resulting in a marked drop of the TOC:TP molar ratio across the trophic transition, with values of 390 ± 60 and 163 ± 8 before and after 1969, respectively (Figure 3). The TOC:TP ratio has been used as a measure of the overall P burial efficiency in sediments, because it accounts for P sink switching during early diagenesis (Anderson et al., 2001). The large drop of the TOC:TP ratio upon fertilization thus implies that the sediments efficiently retained the P added during the fertilization experiment. We further note that the increased sediment burial efficiency of TP was seen for both the epilimnion and hypolimnion, that is, under both oxygenated and (mostly) anoxic bottom waters.

The lower post-1969 molar TFe:TP ratios compared to those before 1969 are also consistent with the enhanced preservation efficiency of P in the sediments after fertilization started (Figure 3). In oxic sediments, where P retention is mainly due to binding to Fe (III) (hydr)oxides, molar TFe:TPe ratios are typically higher than 8 (Jensen et al., 1992). This is the case for the epilimnion sediments below 8-cm depth. At shallower depths, however, the ratios dropped to values of 4–6. In the hypolimnion sediments, the TFe:TP ratios systematically fell below 8 (with the exception of the 13–15-cm interval where the ratio was 8.6). Hence, binding of P by Fe (III) oxides alone does not explain the large enhancements of TP burial during the period of artificial P additions. As elaborated below, we attribute the enhanced post-1969 sedimentary accumulation of P mainly to increased preservation of in-lake produced organic P, as well as a more important sequestration of aqueous phosphate by complexation to humic substances.

4.3. Trophic Transition: P Pools

According to the sequential extraction results, organic P (P_{Org}) formed the largest pool of P in the sediments of Lake 227, with 50 ± 15% of TP present as P_{Org} in both the epilimnion and hypolimnion sediments, and for both the pre- and post-1969 periods (Figures 5 and S4). A dominant role of organic P compounds is also consistent with the P K-edge XANES spectra, which most closely match that of the phytic acid standard (Figure S8). Large contributions of $P_{Org,}$ up to 60%, have been reported for lacustrine sediments (Cao et al., 2009; Rydin, 2000). The small variability of the P_{Org} fraction within the cores further implies that the relative changes in P_{Org} sediment accumulation rates closely followed those of TP. Hence, at the two locations, the P_{Org} accumulation rates increased by more than a factor of 3 after fertilization started. This also caused a distinctive drop in the molar TOC:P_{Org} ratio, on average from around 740 to 330, as the lake switched from the oligotrophic to eutrophic state.

Both the increased P_{Org} accumulation rate and the drop in the TOC:P_{Org} ratio of the sediments deposited after 1969 are ultimately driven by the enhanced deposition of autochthonous algal detritus, relative to terrestrial organic P inputs (Ruttenburg & Goni, 1997). The ^{31}P NMR spectra of the NaOH/EDTA extracts further indicate the presence in the top-most layers of the sediments of organic P compounds and complex inorganic P compounds such as polyphosphates and pyrophosphate (Figure S9). Typically, these condensed P compounds are produced by various microorganisms in response to favorable nutrient conditions, such as those created during the artificial fertilization experiment (Hupfer et al., 1995). In particular, the 0–5 cm depth interval of the epilimnion sediments is enriched in polyphosphate and pyrophosphate (Table 1 and Figure S9). The lower percentage of pyrophosphate in the 0–5 cm interval of the hypolimnion sediments may reflect the frequent occurrence of anoxic bottom waters, which have been shown to promote the release of soluble P through the degradation of condensed P compounds such as polyphosphates (Ahlgren et al., 2006; Gächter et al., 1988; Sannigrahi & Ingall, 2005).

The artificial fertilization of Lake 227 was accompanied by an increase of the fraction of CDB-extractable P, usually identified as P bound to Fe-oxides (P_{Fe}), in the epilimnion sediments but not in the hypolimnion sediments (Figure S4). This is consistent with the corresponding increases in the epilimnion sediments of the TFe concentration and accumulation rate (Figure 4), and with the increase in the fraction of the easily reducible Fe pool (Figures 5 and S5), trends that were not observed in the hypolimnion sediments. Thus, for sediments deposited below the oxygenated bottom waters of the epilimnion, the enhanced accumulation of Fe-oxide-bound P during the fertilization period agrees with the conventional view of a dominant role of

Fe (III) oxides in sequestering P in sediments deposited under well-oxygenated bottom waters (Jensen et al., 1992; Orihel et al., 2017). The abundance of ferric Fe (hydr)oxides in the epilimnion sediments was also confirmed by the Mössbauer spectra (species A, B, C, and D, Table 1).

The decrease in reducible Fe (Fe_{Ox1} + Fe_{Ox2}) in the post-1969 hypolimnion sediments (Figures 5 and S5) is similarly expected, because of the more reducing bottom water conditions. However, even after 1969, reducible Fe (III) continued to represent a major TFe fraction in the hypolimnion sediments and, as a consequence, P_{Fe} remained a small, but not negligible, P sink in the hypolimnion of eutrophic Lake 227. In contrast to the epilimnion sediments, the Mössbauer results suggest that P_{Fe} may comprise phosphate associated to various colloidal Fe (III)-OM complexes, rather than to the commonly invoked Fe (III) oxide minerals, such as goethite and magnetite (Table 1).

For both the epilimnion and hypolimnion sediments, the trophic transition was accompanied by increases in the absolute and relative abundances of P extracted by $NaHCO_3$ (P_{Hum}, Figures 5 and S4). The $NaHCO_3$ extraction releases P associated with soluble organic matter, including humic compounds (Baldwin, 1996). In addition, the extracted P concentrations strongly correlated with the extracted Fe concentrations (Figure S6), while the Fe K-edge XANES spectra of the humate extracts further imply that the humic-associated Fe was in the ferric form (Figure 6). Taken together, these results support the formation and preservation of phosphate-Fe (III)-humic complexes as one of the mechanisms enabling the enhanced TP burial efficiency in the post-1969 sediments (see also, Karlsson et al., 2008; Karlsson & Persson, 2010, 2012; Sundman et al., 2016). However, the larger than unity P:Fe molar ratios in the $NaHCO_3$ extracts (1.6–2.8) requires that other cations, for example, Al^{3+} and Ca^{2+}, provide additional bridging cations between phosphate and the humic compounds (Gerke, 2010).

4.4. Revisiting the Fe-P Connection

Iron clearly plays a more complex role in the sedimentary P cycling of Lake 227 than the classical model of phosphate sorption (desorption) by the oxidative precipitation (reductive dissolution) of Fe (III) (hydr)oxides (see also, Hupfer & Lewandowski, 2008; Joshi et al., 2015; Li et al., 2015). The classical model can in part explain the increased TP accumulation in the post-1969 epilimnion sediments, where a significant increase in easily reducible Fe (hydr)oxides is observed. The Mössbauer spectra of the epilimnion sediments further imply that small particle Fe (III) (hydr)oxides, possibly ferrihydrite or small particle goethite of different particle-size/crystallinity, are intimately associated with organic matter (OM). The complexation of Fe (III) to OM is known to inhibit the polymerization of Fe (III), favoring the formation of smaller, more reactive ferrihydrite particles (Karlsson & Persson, 2012). Thus, P fertilization of Lake 227, and the resulting increased deposition of fresh algal organic matter, may have indirectly created favorable conditions for enhanced retention of P in the epilimnion sediments via sorption of phosphate to ferrihydrite-OM complexes. Organic P compounds may have also bound directly to ferrihydrite, compounds such as DNA and inositol phosphates are known to sorb to sediment minerals (Giles et al., 2015).

Although the Mössbauer spectra also reveal the presence of ferrihydrite-OM complexes in the hypolimnion sediments, these are likely produced in the water column rather than actively forming under the reducing conditions at and below the SWI. One distinctive signature of the lake's transition from oligotrophic to eutrophic state recorded in the hypolimnion sediments was the formation of AVS and pyrite (Figures 5 and S7 and Table 2). As more in-lake-produced algal debris was deposited at the SWI, the contribution of sulfate reduction to OM decomposition increased, which, in turn, released more free sulfide to react with Fe (III) phases (Berner & Raiswell, 1983; Couture et al., 2010). The formation of Fe (II) sulfide mineral phases in the hypolimnion sediments is made possible by the relatively high bottom-water sulfate concentrations (around 22 μM, N. Ansems, unpublished results).

Despite the prevailing anoxic and hypoxic conditions of the hypolimnion, plus the evidence for active sulfate reduction and pyrite formation, most Fe in the post-1969 hypolimnion sediments persisted as oxidized Fe (III). Furthermore, the similarity of the Fe K-edge XANES spectra of the sediments from the pre-1969 (15–20 cm) and post-1969 (0–5 cm) depth intervals (Figure 6) suggests little change in the forms under which Fe (III) was preserved in the organic-rich hypolimnion sediments across the trophic transition. We speculate that the stabilization of Fe (III) may be due to the complexation of Fe (III) to organic matter (Chen et al., 2015; Henneberry et al., 2012), including binding to carboxylic groups of humic compounds (Catrouillet et al., 2014). In turn, the strong association of Fe (III) and sediment OM may promote the formation of phosphate-Fe (III)-humic complexes.

4.5. Sediment P Accumulation and Internal Loading

Prior to the start of the fertilization experiment, the external TP load to Lake 227 was estimated at 5.3 kg yr^{-1} (Figure 8), which amounts to an annual TP load of about 100 mg P per m^2 of lake surface area. This value falls within the 22–114 mg P m^{-2} yr^{-1} range reported for ELA's Lakes 442 and 373 (Campbell, 1994). Atmospheric deposition further accounts for most (70%) of the TP input to the pristine lake, in large part supplied as nutrient-rich conifer pollen from the surrounding forest (Doskey & Talbot, 2000; Graham et al., 2006; Lee & Booth, 2003). In small boreal oligotrophic lakes, a significant portion of the productive capacity is often sustained by pollen deposited during the summer months, with up to 60% of the pollen TP released as soluble and bioavailable P to the water column (Doskey & Ugoagwu, 1989; Graham et al., 2006).

The artificial fertilization of Lake 227 increased the external P load by more than a factor of five, causing the pristine, oligotrophic lake to switch to eutrophic conditions characterized by algal blooms. The results of this fertilization experiment led to the general acceptance that reductions in external P loading are a primary measure in lake water-quality restoration efforts (Mohamed et al., 2019). However, studies often report a delay in water-quality recovery when such reductions are implemented, with timelines of up to 20 years (Søndergaard et al., 2005), 20–25 years (Dørge & Windolf, 2003), and even longer than 50 years (Carpenter, 2005). A major cause for the delayed response to the external P load reduction is "internal P loading," that is, the efflux of soluble reactive P from sediments generated from the remobilization of P accumulated during periods of high external P loading (Søndergaard et al., 2002).

Of the TP input to the pre-1969 lake, an estimated 89%, or 4.7 kg P yr^{-1}, remained buried in the sediments (Figure 8), primarily in organic forms (Figure 5). With the onset of the fertilization experiment, sediment P accumulation rose to 26.8 kg P yr^{-1} or 22.1 kg P yr^{-1} more than before fertilization (Figure 8). This extra accumulation represents 92% of the artificially added P (24 kg P yr^{-1}). This large sediment P reservoir is composed of reactive P phases that could sustain internal P loading over an extended period of time. A rough estimate of the corresponding time scale is derived as follows:

The pore water total dissolved P (TDP) gradients just below the SWI measured in the 2011 cores (Figure S1) imply a much larger efflux of TDP from the hypolimnion than epilimnion sediments, presumably because of the efficient trapping of TDP by Fe (III) (hydr)oxides in the upper sediments of the epilimnion (section 4.4). From the measured pore water gradients and sediment porosity plus the temperature-corrected molecular diffusion coefficient, diffusive benthic fluxes of TDP can be calculated (Van Cappellen & Gaillard, 2019). This yields a whole-lake average P efflux of 0.62 μmol cm^{-2} yr^{-1}. This efflux is primarily driven by the legacy sediment P accumulated since fertilization started, because under natural, non-fertilized conditions the flux would be orders of magnitude lower (Orihel et al., 2017).

The amount of sediment P accumulation due to the artificial fertilization during the 43 years between the start of fertilization (1969) and the 2011 core retrieval is calculated from the average extra sediment P accumulation rate (22.1 kg P yr^{-1}) multiplied by the number of years. Normalized to the sediment surface area of the lake, this yields a legacy mass of 1.8 mg P cm^{-2}, or 58 μmol P cm^{-2}. Assuming a first-order dependence of the TDP efflux from the sediment on the legacy P mass in the sediments, the corresponding half-life of legacy P is then 66 years.

The estimated half-life must be taken with a high degree of caution, not only because of the assumed first-order kinetic dependence, which lumps various P forms together, but also because it relies on a single time point estimation of the benthic TDP efflux, which may or may not be representative of the annually-averaged internal P loading. Nevertheless, the estimated half-life would suggest that internal P loading due to the accumulated legacy P could help sustain relatively high in-lake productivity over several decades, even after the external P loading would be reduced to its pre-1969 level. This result agrees with the delay time scales in lake recovery mentioned earlier in this section, as well as recent process-based modeling of the internal P loading response to restoration efforts (Markelov et al., 2019).

5. Conclusions

The artificial fertilization experiment of Lake 227 has yielded ground-breaking insights into the role of phosphorus as a limiting nutrient of lake productivity (Schindler, 2009). These insights, in turn, have informed lake restoration and management efforts around the world. Here, we report on the changes in sediment accumulation and speciation of P and associated elements, including C, Fe, and S, which accompanied the rapid transition of Lake 227 from oligotrophic to eutrophic conditions. In particular, the sediment TOC and TP concentrations and accumulation rates experienced many-fold increases with the onset of experimental eutrophication. The extra TP accumulation accounts for 92% of the artificially-added P since fertilization began, nearly equally divided between the sediments underlying the epilimnion and hypolimnion.

Phosphorus bound in organic compounds (P_{org}) forms the largest pool of sedimentary P, staying relatively stable at ~50% of TP before and after the onset of artificial fertilization. The largest relative change in sediment P burial associated with the lake's eutrophication is the increased importance of $NaHCO_3$-extractable P (P_{Hum}). The positive correlations between P and Fe extracted by $NaHCO_3$, plus the dominance of Fe (III) inferred from the Mössbauer and XANES data, are consistent with the enhanced formation and preservation in the sediments of phosphate-metal-humic complexes, with Fe (III) as one of the bridging cations. The persistence of Fe (III), even under the highly reducing conditions of the bottom waters of the hypolimnion, likely reflects stabilization by Fe (III) binding to organic matter. Nonetheless, in the hypolimnion sediments the increased deposition and oxidative degradation of in-lake produced algal matter causes some of the sedimentary Fe to be sequestered as Fe (II) sulfides, including pyrite. Further research into the observed changes in the sedimentary distributions of the various P and Fe pools should also consider the potential changes in the lateral, and possibly recursive, nearshore-offshore exchanges of water column solutes and particulate matter that accompanied the increased production and degradation of algal biomass in Lake 227 after 1969.

Overall, our results show that the P additions to Lake 227 since 1969 are primarily stored in the lake's sediments under relatively reactive forms, that is, in-lake-produced organic P compounds, including condensed P compounds, phosphate sorbed to Fe (III) (hydroxides) and phosphate-metal-humic complexes. This large legacy of reactive P may potentially fuel internal P loading to the water column on time scales of decades, once artificial fertilization is terminated. The confounding role of sediment legacy P needs to be recognized when assessing the effectiveness of measures taken to reverse the negative impacts of cultural eutrophication.

Acknowledgments

The authors acknowledge the insightful comments and suggestions of two journal reviewers. Financial support for this research was provided by the Canadian Excellence Research Chair (CERC) Program. The authors also wish to thank the IISD Experimental Lakes Area (ELA) of Northern Ontario for providing field site access, sampling equipment, and on-site laboratory facilities. Especially, we acknowledge ELA scientists and staff responsible for the artificial fertilization of Lake 227 over the past 50 years, with particular mention to David Schindler, Michael Paterson, and Lewis Molot. The Environmental Molecular Sciences Laboratory (EMSL) is acknowledged. EMSL is a user facility funded by the U.S. Department of Energy's Office of Biological and Environmental Research and located at Pacific Northwest National Laboratory. We are grateful for the assistance of Corey Liu at the Stanford Magnetic Resonance Laboratory for the P-NMR analysis. The Canadian Light Source is financially supported by NSERC, NRC, CIHR, and the University of Saskatchewan.

Data Availability Statement

Readers can access open source data in the 4TU.Centre for Research Data.

References

Ahlgren, J., Reitzel, K., Danielsson, R., Gogoll, A., & Rydin, E. (2006). Biogenic phosphorus in oligotrophic mountain lake sediments: Differences in composition measured with NMR spectroscopy. *Water Research*, *40*(20), 3705–3712. https://doi.org/10.1016/j.watres.2006.09.006

Ahlgren, J., Tranvik, L., Gogoll, A., Waldebäck, M., Markides, K., & Rydin, E. (2005). Sediment depth attenuation of biogenic phosphorus compounds measured by ^{31}P NMR. *Envrionmental Science & Technology*, *39*(3), 867–872. https://doi.org/10.1021/es049590h

Anderson, L. D., Delaney, M. L., & Faul, K. L. (2001). Carbon to phosphorus ratios in sediments: Implications for nutrient cycling. *Global Biogeochemical Cycles*, *15*(1), 65–79. https://doi.org/10.1029/2000GB001270

Appleby, P. G., Birks, H. H., Flower, R. J., Rose, N., Peglar, S. M., Ramdani, M., & Fathi, A. (2001). Radiometrically determined dates and sedimentation rates for recent sediments in nine North African wetland lakes (the CASSARINA project). *Aquatic Ecology*, *35*(3/4), 347–367. https://doi.org/10.1023/A:1011938522939

Baldwin, D. S. (1996). The phosphorus composition of a diverse series of Australian sediments. *Hydrobiologia*, *335*(1), 63–73. https://doi.org/10.1007/BF00013684

Barber, A., Brandes, J., Leri, A., Lalonde, K., Balind, K., Wirick, S., et al. (2017). Preservation of organic matter in marine sediments by inner-sphere interactions with reactive iron. *Scientific Reports*, *7*(1), 366. https://doi.org/10.1038/s41598-017-00494-0

Beauchemin, S., Hesterberg, D., Chou, J., Beauchemin, M., Simard, R. R., & Sayers, D. E. (2003). Speciation of phosphorus in phosphorus-enriched agricultural soils using X-ray absorption near-edge structure spectroscopy and chemical fractionation. *Journal of Environmental Quality*, *32*(5), 1809–1819. https://doi.org/10.2134/jeq2003.1809

Berner, R. A., & Raiswell, R. (1983). Burial of organic carbon and pyrite sulfur in sediments over Phanerozoic time: A new theory. *Geochimica et Cosmochimca Acta*, *47*(5), 855–862. https://doi.org/10.1016/0016-7037(83)90151-5

Bhattacharyya, A., Campbell, A. N., Tfaily, M. M., Lin, Y., Kukkadapu, R. K., Silver, W. L., et al. (2018). Redox fluctuations control the coupled cycling of iron and carbon in tropical forest soils. *Environmental Science & Technology*, *52*(24), 14129–14139. https://doi.org/10.1021/acs.est.8b03408

Borch, T., Kretzschmar, R., Kappler, A., Van Cappellen, P., Ginder-Vogel, M., Voegelin, A., & Campbell, K. (2010). Biogeochemical redox processes and their impact on contaminant dynamics. *Environmental Science & Technology*, *44*(1), 15–23. https://doi.org/10.1021/es9026248

Brunskill, G. J., & Schindler, D. W. (1971). Geography and bathymetry of selected lake basins in the Experimental Lakes area (ELA), northwestern Ontario. *Journal of the Fisheries Research Board of Canada*, *28*(2), 139–155. https://doi.org/10.1139/f71-028

Burdige, D. J. (2007). Preservation of organic matter in marine sediments: Controls, mechanisms, and an imbalance in sediment organic carbon budgets? *Chemical Reviews*, *107*(2), 467–485. https://doi.org/10.1021/cr050347q

Burton, E. D., Sullivan, L. A., Bush, R. T., Johnston, S. G., & Keene, A. F. (2008). A simple and inexpensive chromium-reducible sulfur method for acid-sulfate soils. *Applied Geochemistry*, *23*(9), 2759–2766. https://doi.org/10.1016/j.apgeochem.2008.07.007

Cade-Menun, B. J. (2015). Improved peak identification in ^{31}P-NMR spectra of environmental samples with a standardized method and peak library. *Geoderma*, *257-258*, 102–114. https://doi.org/10.1016/j.geoderma.2014.12.016

Cade-Menun, B. J., & Preston, C. M. (1996). A comparison of soil extraction procedures for ^{31}P NMR spectroscopy. *Soil Science*, *161*(11), 770–785. https://doi.org/10.1097/00010694-199611000-00006

Campbell, P. (1994). Phosphorus budgets and stoichiometry during the open-water season in two unmanipulated lakes in the Experimental Lakes Area, northwestern Ontario. *Canadian Journal of Fisheries and Aquatic Sciences*, *51*(12), 2739–2755. https://doi.org/10.1139/f94-275

Cao, X., Song, C., Zhou, Y., Strojsova, A., Znachor, P., Zopmelova, E., & Vrba, J. (2009). Extracellular phosphatases produced by phytoplankton and other sources in shallow eutrophic lakes (Wuhan, China): Taxon-specific versus bulk activity. *Limnology*, *10*(2), 95–104. https://doi.org/10.1007/s10201-009-0265-9

Caraco, N. F., Cole, J. J., & Likens, G. E. (1991). Phosphorus release from anoxic sediments: Lakes that break the rules. *Verhandlungen des Internationalen Verein Limnologie*, *24*, 2985–2988.

Carpenter, S. R. (2005). Eutrophication of aquatic ecosystems: Bistability and soil phosphorus. *Proceedings of the National Academy of Sciences of the United States of America*, *102*(29), 10002–10005. https://doi.org/10.1073/pnas.0503959102

Catrouillet, C., Davranche, M., Dia, A., Bouhnik-Le Coz, M., Marsac, R., Pourret, O., & Gruau, G. (2014). Geochemical modeling of Fe (II) binding to humic and fulvic acids. *Chemical Geology*, *372*, 109–118. https://doi.org/10.1016/j.chemgeo.2014.02.019

Chen, C., Kukkadapu, R. L., & Sparks, D. L. (2015). Influence of coprecipitated organic matter on Fe^{2+}(aq)-catalyzed transformation of ferrihydrite: Implications of carbon dynamics. *Environmental Science & Technology*, *49*(18), 10927–10936. https://doi.org/10.1021/acs.est.5b02448

Couture, R. M., Gobeil, C., & Tessier, A. (2010). Arsenic, iron and sulfur co-diagenesis of in lake sediments. *Geochimica et Cosmochimica Acta*, *74*(4), 1238–1255. https://doi.org/10.1016/j.gca.2009.11.028

Dillon, P. J., & Molot, L. A. (1997). Effect of landscape form on export of dissolved organic carbon, iron, and phosphorus from forested stream catchments. *Water Resources Research*, *33*(11), 2591–2600. https://doi.org/10.1029/97WR01921

Dillon, P. J., & Rigler, F. H. (1975). A simple method for predicting the capacity of a lake for development based on lake trophic status. *Journal of the Fisheries Research Board of Canada*, *32*(9), 1519–1531. https://doi.org/10.1139/f75-178

Dørge, J., & Windolf, J. (2003). Implementation of the water framework directive—Can we use models as a tool in integrated river management? *International Journal of River Basin Management*, *1*(2), 165–171. https://doi.org/10.1080/15715124.2003.9635203

Doskey, P. V., & Talbot, R. W. (2000). Sediment chronologies of atmospheric deposition in a precipitation-dominated seepage lake. *Limnology and Oceanography*, *45*(4), 895–904. https://doi.org/10.4319/lo.2000.45.4.0895

Doskey, P. V., & Ugoagwu, B. J. (1989). Atmospheric deposition of macronutrients by pollen at a semi-remote site in northern Wisconsin. *Atmospheric Environment*, *23*(12), 2761–2766. https://doi.org/10.1016/0004-6981(89)90556-8

Emerson, S., & Hesslein, R. (1973). Distribution and uptake of artificially introduced Radium-226 in a small lake. *Canadian Journal of Fisheries and Aquatic Sciences*, *30*, 1485–1490.

Gächter, R., Meyer, J. S., & Mares, A. (1988). Contribution of bacteria to release and fixation of phosphorus in lake sediments. *Limnology and Oceanography*, *33*, 1542–1558.

Gächter, R., & Müller, B. (2003). Why the phosphorus retention of lakes does not necessarily depend on the oxygen supply to their sediment surface. *Limnology and Oceanography*, *48*(2), 929–933. https://doi.org/10.4319/lo.2003.48.2.0929

Gerke, J. (2010). Humic (organic matter)-Al (Fe)-phosphate complexes: An underestimated phosphate form in soils and source of plant-available phosphate. *Soil Science*, *175*(9), 417–425. https://doi.org/10.1097/SS.0b013e3181f1b4dd

Giles, C. D., Lee, L. G., Cade-Menun, B. J., Hill, J. E., Isles, P. D. F., Schroth, A. W., & Druschel, G. K. (2015). Characterization of organic phosphorus form and bioavailability in lake sediments using ^{31}P nuclear magnetic resonance and enzymatic hydrolysis. *Journal of Environmental Quality*, *44*(3), 882–894. https://doi.org/10.2134/jeq2014.06.0273

Graham, M. D., Vinebrooke, R. D., & Turner, M. (2006). Coupling of boreal forests and lakes: Effects of conifer pollen on littoral communities. *Limnology and Oceanography*, *51*(3), 1524–1529. https://doi.org/10.4319/lo.2006.51.3.1524

Guardado, I., Urrutia, O., & García-Mina, J. M. (2007). Size distribution, complexing capacity, and stability of phosphate-metal-humic complexes. *Journal of Agricultural and Food Chemistry*, *55*(2), 408–413. https://doi.org/10.1021/jf062894y

Guardado, I., Urrutia, O., & Garcia-Mina, J. M. (2008). Some structural and electronic features of the interaction of phosphate with metal-humic complexes. *Journal of Agricultural and Food Chemistry*, *56*(3), 1035–1042. https://doi.org/10.1021/jf072641k

Hall, R. I., Wolfe, B. B., Wiklund, J. A., Edwards, T. W. D., Farwell, A. J., & Dixon, D. G. (2012). Has Alberta oil sands development altered delivery of polycyclic aromatic compounds to the Peace-Athabasca Delta? *PLoS ONE*, *7*(9), e46089. https://doi.org/10.1371/journal.pone.0046089

He, Z., Olk, D. C., & Cade-Menun, B. J. (2011). Forms and lability of phosphorus in humic acid fractions of hord silt loam soil. *Soil Science Society of America Journal*, *75*(5), 1712–1722. https://doi.org/10.2136/sssaj2010.0355

Henneberry, Y. K., Kraus, T. E. C., Nico, P. S., & Horwath, W. R. (2012). Structural stability of co-precipitated natural organic matter and ferric iron under reducing conditions. *Organic Geochemistry*, *48*, 81–89. https://doi.org/10.1016/j.orggeochem.2012.04.005

Ho, E. S., & Meyers, P. A. (1994). Variability of early diagenesis in lake-sediments—Evidence from the sedimentary geolipid record in an isolated tarn. *Chemical Geology*, *112*(3-4), 309–324. https://doi.org/10.1016/0009-2541(94)90031-0

Hupfer, M., Gächter, R., & Rüegger, H. (1995). Polyphosphate in lake sediments: ^{31}P NMR spectroscopy as a tool for its identification. *Limnology and Oceanography*, *40*(3), 610–617. https://doi.org/10.4319/lo.1995.40.3.0610

Hupfer, M., & Lewandowski, J. (2008). Oxygen controls the phosphorus release from lake sediments—A long-lasting paradigm in limnology. *International Review of Hydrobiology*, *93*(4-5), 415–432. https://doi.org/10.1002/iroh.200711054

Jensen, H. S., Kristensen, P., Jeppesen, E., & Skytthe, A. (1992). Iron:phosphorus ratio in surface sediment as an indicator of phosphate release from aerobic sediments in shallow lakes. *Hydrobiologia*, *235*(236), 731–743.

Jeppesen, E., Søndergaard, M., Jensen, J. P., Havens, K., Anneville, O., & Carvalho, L. (2005). Lake responses to reduced nutrient loading: An analysis of contemporary long-term data from 35 case studies. *Freshwater Biology*, *50*(10), 1747–1771. https://doi.org/10.1111/j.1365-2427.2005.01415.x

Joshi, S. R., Kukkadapu, R. K., Burdige, D. J., Bowden, M. E., Sparks, D. L., & Jaisi, D. P. (2015). Organic matter remineralization predominates phosphorus cycling in the mid-bay sediments in the Chesapeake Bay. *Environmental Science & Technology*, *49*(10), 5887–5896. https://doi.org/10.1021/es5059617

Jung, A. V., Chanudet, V., Lartiges, B. S., Ghabaja, J., Abdelmoula, M., & Bersillon, J. L. (2012). Association of iron oligomeric species with natural organic matter: A combined EELS and Mosssbaeur investigation. *Aquatic Sciences*, *74*(4), 769–779. https://doi.org/10.1007/s00027-012-0260-9

Karlsson, T., & Persson, P. (2010). Coordination chemistry and hydrolysis of Fe (III) in a peat humic acid studied by X-ray absorption spectroscopy. *Geochimica et Cosmochimica Acta*, *74*(1), 30–40. https://doi.org/10.1016/j.gca.2009.09.023

Karlsson, T., & Persson, P. (2012). Complexes with aquatic organic matter suppress hydrolysis and precipitation of Fe (III). *Chemical Geology*, *322-323*, 19–27. https://doi.org/10.1016/j.chemgeo.2012.06.003

Karlsson, T., Persson, P., Skyllberg, U., Mörth, C. M., & Giesler, R. (2008). Characterisation of iron (III) in organic soils using extended X-ray absorption fine structure spectroscopy. *Environmental Science & Technology*, *42*(15), 5449–5454. https://doi.org/10.1021/es800322j

Kleeberg, A., Freidank, A., & Jöhnk, K. (2013). Effects of ice cover on sediment resuspension and phosphorus entrainment in shallow lakes: Combining in situ experiments and wind-wave modelling. *Limnology and Oceanography*, *58*(5), 1819–1833. https://doi.org/10.4319/lo.2013.58.5.1819

Lalonde, K., Mucci, A., Quellet, A., & Gelinas, Y. (2012). Preservation of organic matter in sediments promoted by iron. *Nature*, *483*(7388), 198–200. https://doi.org/10.1038/nature10855

Lee, E. J., & Booth, T. (2003). Macronutrient input from pollen in two regenerating pine stands in Southeast. *Korea Ecological Research*, *18*(4), 423–430. https://doi.org/10.1046/j.1440-1703.2003.00566.x

Levine, S. N., & Schindler, D. W. (1980). Radiochemical analysis of orthophosphate concentration and seasonal changes in the flux of orthophosphate to seston in two Canadian shield lakes. *Canadian Journal for Fisheries and Aquatic Sciences*, *37*(3), 479–487. https://doi.org/10.1139/f80-062

Li, J., Bai, Y., Bear, K., Joshi, S., & Jaisi, D. (2017). Phosphorus availability and turnover in the Chesapeake Bay: Insights from nutrient stoichiometry and phosphate oxygen isotope ratios. *Journal of Geophysical Research – Biogeosciences*, *122*(4), 811–824. https://doi.org/10.1002/2016JG003589

Li, W., Joshi, S. R., Hou, G., Burdige, D. J., Sparks, D. L., & Jaisi, D. P. (2015). Characterizing phosphorus speciation of Chesapeake Bay sediments using chemical extraction, ^{31}P NMR, and X-ray absorption fine structure spectroscopy. *Envrionmental Science & Technology*, *49*(1), 203–211. https://doi.org/10.1021/es504648d

Malley, D. F., & Mills, K. H. (1992). Whole-lake experimentation as a tool to assess ecosystem health, response to stress and recovery: The Experimental Lakes Area experience. *Journal of Aquatic Ecosystem Science*, *1*(3), 159–174. https://doi.org/10.1007/BF00044713

Markelov, I., Couture, R. M., Fisher, R., Haande, S., & Van Cappellen, P. (2019). Coupling water column and sediment biogeochemical dynamics: Modeling internal phosphorus loading, climate change responses and mitigation measures in Lake Vansjø, Norway. *Journal of Geophysical Research – Biogeosciences*, *124*(12), 3847–3866. https://doi.org/10.1029/2019JG005254

Meinikmann, K., Hupfer, M., & Lewandowski, J. (2015). Phosphorus in groundwater discharge - a potential source for lake eutrophication. *Journal of Hydrology*, *524*, 214–226. https://doi.org/10.1016/j.jhydrol.2015.02.031

Mohamed, N. M., Wellen, C., Parsons, C. T., Taylor, W. D., Arhonditsis, G., Chomicki, K. M., et al. (2019). Understanding and managing the re-eutrophication of Lake Erie: Knowledge gaps and research priorities. *Freshwater Science*, *38*(4), 675–691. https://doi.org/10.1086/705915

Monaghan, E. J., & Ruttenburg, K. C. (1999). Dissolved organic phosphorus in the coastal ocean: Reassessment of available methods and seasonal phosphorus profiles from the Eel River shelf. *Limnology and Oceanography*, *44*(7), 1702–1714. https://doi.org/10.4319/lo.1999.44.7.1702

Mortimer, C. H. (1941). The exchange of dissolved substances between mud and water in lakes. *Journal of Ecology*, *29*(2), 280–329. https://doi.org/10.2307/2256395

Murphy, J., & Riley, J. P. (1962). A modified single solution method for the determination of phosphate in natural waters. *Analytica Chimica Acta*, *27*, 31–36. https://doi.org/10.1016/S0003-2670(00)88444-5

O'Connell, D. W., Mark Jensen, M., Jakobsen, R., Thamdrup, B., Andersen, T. J., Kovacs, A., & Bruun Hansen, H. C. (2015). Vivianite formation and its role in phosphorus retention in Lake Ørn, Denmark. *Chemical Geology*, *409*, 42–53. https://doi.org/10.1016/j.chemgeo.2015.05.002

Orihel, D. M., Baulch, H. M., Casson, N. J., North, R. L., Parsons, C. T., Seckar, D. C. M., & Venkiteswaran, J. J. (2017). Internal phosphorus loading in Canadian fresh waters: A critical review and data analysis. *Canadian Journal of Fisheries and Aquatic Sciences*, *74*(12), 2005–2029. https://doi.org/10.1139/cjfas-2016-0500

Parker, B. R., Schindler, D. W., Beaty, K. G., Stainton, M. P., & Kasian, S. E. M. (2009). Long-term changes in climate, streamflow, and nutrient budgets for first-order catchments at the Experimental Lakes Area (Ontario, Canada). *Canadian Journal of Fisheries and Aquatic Sciences*, *66*(11), 1848–1863. https://doi.org/10.1139/F09-149

Peretyazhko, T., Zachara, J. M., Kukkadapu, R. K., Heald, S. M., Kutnyakov, I. V., Resch, C. T., et al. (2012). Pertechnetate (TcO_4^-) reduction by reactive ferrous iron forms in naturally anoxic, redox transition zone sediments from the Hanford Site, USA. *Geochimica et Cosmochimica Acta*, *92*, 48–66. https://doi.org/10.1016/j.gca.2012.05.041

Poulton, S. W., & Canfield, D. E. (2005). Development of a sequential extraction procedure for iron: Implications for iron partitioning in continentally derived particulates. *Chemical Geology*, *214*(3–4), 209–221. https://doi.org/10.1016/j.chemgeo.2004.09.003

Rancourt, D., & Ping, J. (1991). Voigt-based methods for arbitrary-shape static hyperfine parameter distributions in Mössbauer spectroscopy. *Nuclear Instruments and Methods in Physics Research Section B: Beam Interactions with Materials and Atoms*, *58*(1), 85–97. https://doi.org/10.1016/0168-583X(91)95681-3

Ravel, B., & Newville, M. (2005). ATHENA, ARTEMIS, HEPHAESTUS: Data analysis for X-ray absorption spectroscopy using IFEFFIT. *Journal of Synchrotron Radiation*, *12*(4), 537–541. https://doi.org/10.1107/S0909049505012719

Read, E. K., Ivancic, M., Hanson, P., Cade-Menun, B. J., & McMahon, K. D. (2014). Phosphorus speciation in a eutrophic lake by ^{31}P NMR spectroscopy. *Water Research*, *62*, 229–240. https://doi.org/10.1016/j.watres.2014.06.005

Riggle, J., & Von Wandruszka, R. (2005). Binding of inorganic phosphate to dissolved metal humates. *Talanta*, *66*(2 SPEC. ISS.), 372–375. https://doi.org/10.1016/j.talanta.2004.11.003

Ruttenberg, K. C. (1992). Development of a sequential extraction method for different forms of phosphorus in marine sediments. *Limnology and Oceanography*, *37*(7), 1460–1482. https://doi.org/10.4319/lo.1992.37.7.1460

Ruttenburg, K. C., & Goni, M. A. (1997). Phosphorus distribution, C:N:P ratios, and $\delta^{13}C(OC)$ in arctic, temperate, and tropical coastal sediments: Tools for characterizing bulk sedimentary organic matter. *Marine Geology*, *139*(1–4), 123–145. https://doi.org/10.1016/S0025-3227(96)00107-7

Rydin, E. (2000). Potentially mobile phosphorus in Lake Erken sediment. *Water Research*, *34*(7), 2037–2042. https://doi.org/10.1016/S0043-1354(99)00375-9

Sannigrahi, P., & Ingall, E. (2005). Polyphosphates as a source of enhanced P fluxes in marine sediments overlain by anoxic waters: Evidence from ^{31}P NMR. *Geochemical Transactions*, *6*(3), 52–59. https://doi.org/10.1186/1467-4866-6-52

Schindler, D., Heckey, R. E., Findlay, D. L., et al. (2008). Eutrophication of lakes cannot be controlled by reducing nitrogen input: Results of a 37-year whole-ecosystem experiment. *Proceedings of the National Academy of Sciences*, *105*(32), 11254–11258. https://doi.org/10.1073/pnas.0805108105

Schindler, D. W. (1971). Carbon, nitrogen, phosphorus and the eutrophication of freshwater lakes. *Journal of Phycology*, *7*, 321–329.

Schindler, D. W. (2009). A personal history of the experimental lakes project. *Canadian Journal of Fisheries and Aquatic Sciences*, *66*(11), 1837–1847. https://doi.org/10.1139/F09-134

Schindler, D. W., Hesslein, R. H., & Turner, M. A. (1987). Exchange of nutrients between sediments and water after 15 years of experimental eutrophication. *Canadian Journal of Fisheries and Aquatic Sciences*, *44*(1), 26–33.

Schroth, A. W., Giles, C. D., Isles, P. D. F., Xu, Y., Perzan, Z., & Druschel, G. K. (2015). Dynamic coupling of iron, manganese, and phosphorus behavior in water and sediment of shallow ice-covered eutrophic lakes. *Envrionmental Science & Technology*, *49*(16), 9758–9767. https://doi.org/10.1021/acs.est.5b02057

Shao, H., Kukkadapu, R. K., Krogstad, E. J., Newburn, M. K., & Cantrell, K. J. (2014). Mobilization of metals from Eau Claire siltstone and the impact of oxygen under geological carbon dioxide sequestration conditions. *Geochimica et Cosmochimica Acta*, *141*, 62–82. https://doi.org/10.1016/j.gca.2014.06.011

Shaw, R., Trimbee, A., Minty, A., Fricker, H., & Prepas, E. (1989). Atmospheric deposition of phosphorus and nitrogen in central Alberta with emphasis on Narrow Lake. *Water, Air, & Soil Pollution*, *43*(1-2), 119–134. https://doi.org/10.1007/BF00175588

Sobek, S., Söderbäck, B., Karlsson, S., Andersson, E., & Brunberg, A. K. (2006). A carbon budget of a small humic lake: An example of the importance of lakes for organic matter cycling in boreal catchments. *Ambio*, *35*(8), 469–475. https://doi.org/10.1579/0044-7447(2006)35[469:ACBOAS]2.0.CO;2

Søndergaard, M., Jensen, J. P., & Jeppesen, E. (2005). Seasonal response of nutrients to reduced phosphorus loading in 12 Danish lakes. *Freshwater Biology*, *50*(10), 1605–1615. https://doi.org/10.1111/j.1365-2427.2005.01412.x

Søndergaard, M., Jensen, J. P., Jeppesen, E., & Hald Møller, P. (2002). Seasonal dynamics in the concentrations and retention of phosphorus in shallow Danish lakes after reduced loading. *Aquatic Ecosystem Health & Management*, *5*(1), 19–29. https://doi.org/10.1080/14634980260199936

Sundman, A., Karlsson, T., Sjöberg, S., & Persson, P. (2016). Impact of iron-organic matter complexes on aqueous phosphate concentrations. *Chemical Geology*, *426*, 109–117. https://doi.org/10.1016/j.chemgeo.2016.02.008

Tipping, E., Benham, S., Boyle, J. F., Crow, P., Davies, J., Fischer, U., et al. (2014). Atmospheric deposition of phosphorus to land and freshwater. *Environmental Science: Processes and Impacts*, *16*, 1608–1617. https://doi.org/10.1039/c3em00641g

Toor, G. S., Hunger, S., Peak, J. D., Sims, J. T., & Sparks, D. L. (2006). Advances in the characterization of phosphorus in organic wastes: Environmental and agronomic applications. *Advances in Agronomy*, *89*, 1–72. https://doi.org/10.1016/S0065-2113(05)89001-7

Van Cappellen, P., & Gaillard, J. F. (2019). Biogeochemical dynamics in aquatic sediments. In *Reactive transport in porous media* (pp. 335–376). Germany: Walter de Gruyter GmbH.

Van der Molen, D. T., & Boers, P. C. N. (1994). Influence of internal loading on phosphorus concentration in shallow lakes before and after reduction of the external loading. *Hydrobiologia*, *275*(276), 379–389.

Watanabe, F. S., & Olsen, S. R. (1962). Colorimetric determination of phosphorus in water extracts of soils. *Soil Science*, *93*(3), 183–188. https://doi.org/10.1097/00010694-196203000-00005

Welch, E. B., & Cooke, G. D. (2005). Internal phosphorus loading in shallow lakes: Importance and control. *Lake and Reservoir Management*, *21*(2), 209–217. https://doi.org/10.1080/07438140509354430

Zhao, J., Huggins, F., Feng, Z., & Huffman, G. P. (1996). Surface-induced superparamagnetic relaxation in nanoscale ferrihydrite particles. *Physical Review B*, *54*(5), 3403–3407. https://doi.org/10.1103/PhysRevB.54.3403

Erratum

In the originally published version of this article, Figure 1 published without panels a and b. The figure has since been corrected, and this version may be considered the authoritative version of record.